

Broad Absorption Line Variability in Radio-Loud Quasars

C. A. Welling,¹ B. P. Miller,^{2,3} W. N. Brandt,^{4,5} D. M. Capellupo,^{6,7} & R. R. Gibson⁸

¹*Department of Physics and Astronomy, Dickinson College, Carlisle, PA 17013*

²*Department of Astronomy, University of Michigan, 500 Church Street, Ann Arbor, MI 48109*

³*Department of Physics and Astronomy, Macalester College, 1600 Grand Ave, Saint Paul, MN 55105*

⁴*Department of Astronomy and Astrophysics, The Pennsylvania State University, 525 Davey Laboratory, University Park, PA 16802*

⁵*Institute for Gravitation and the Cosmos, The Pennsylvania State University, University Park, PA 16802*

⁶*Department of Astronomy, University of Florida, 211 Bryant Space Science Center, Gainesville, FL 32611*

⁷*School of Physics and Astronomy, Tel Aviv University, Tel Aviv 69978, Israel*

⁸*Department of Astronomy, University of Washington, Box 351580, Seattle, WA 98195*

24 March 2021

ABSTRACT

We investigate C IV broad absorption line (BAL) variability within a sample of 46 radio-loud quasars (RLQs), selected from SDSS/FIRST data to include both core-dominated (39) and lobe-dominated (7) objects. The sample consists primarily of high-ionization BAL quasars, and a substantial fraction have large BAL velocities or equivalent widths; their radio luminosities and radio-loudness values span ~ 2.5 orders of magnitude. We have obtained 34 new Hobby-Eberly Telescope (HET) spectra of 28 BAL RLQs to compare to earlier SDSS data, and we also incorporate archival coverage (primarily dual-epoch SDSS) for a total set of 78 pairs of equivalent width measurements for 46 BAL RLQs, probing rest-frame timescales of ~ 80 –6000 d (median 500 d). In general, only modest changes in the depths of segments of absorption troughs are observed, akin to those seen in prior studies of BAL RQQs. Also similar to previous findings for RQQs, the RLQs studied here are more likely to display BAL variability on longer rest-frame timescales. However, typical values of $|\Delta EW|$ and $|\Delta EW|/\langle EW \rangle$ are $\sim 40 \pm 20\%$ lower for BAL RLQs when compared with those of a timescale-matched sample of BAL RQQs. Optical continuum variability is of similar amplitude in BAL RLQs and BAL RQQs; for both RLQs and RQQs, continuum variability tends to be stronger on longer timescales. BAL variability in RLQs does not obviously depend upon their radio luminosities or radio-loudness values, but we do find tentative evidence for greater fractional BAL variability within lobe-dominated RLQs. Enhanced BAL variability within more edge-on (lobe-dominated) RLQs supports some geometrical dependence to the outflow structure.

Key words: galaxies: active — galaxies: jets — quasars: absorption lines

1 INTRODUCTION

Accretion in quasars appears to lead naturally to the formation of outflows that may regulate supermassive black hole growth and provide feedback to the host galaxy (e.g., Arav et al. 2013 and references therein), potentially helping to quench star formation. In radio-quiet quasars (RQQs) such outflows are most readily apparent as broad absorption lines (BALs; Weymann et al. 1981, 1991) found blueward¹ of UV emission lines; these features can occur at a wide range of velocities (to greater than $0.1c$) and are ob-

served in 10–20% of optically selected quasars (e.g., Hewett & Foltz 2003). The “orientation” model hypothesizes that BALs are common to RQQs but only apparent over a limited range of inclinations to the line of sight. (While successful at explaining many observed properties of BAL and non-BAL quasars, this simple model may not capture the full physical complexity of outflow generation and structure.) The prevalence of velocity structure within C IV BALs that matches the Ly α –N V velocity offset (Weymann et al. 1991; Arav & Begelman 1994) indicates that these BAL outflows are radiatively accelerated, as does the correlation between maximum outflow velocity and UV luminosity (Laor & Brandt 2002; Ganguly et al. 2007). Simulations (e.g., Proga et al. 2000) demonstrate that winds can be driven off a classical accre-

¹ A rare handful of quasars display redshifted BALs, perhaps from an infall or a rotating outflow (Hall et al. 2013).

tion disk, with interior “shielding gas” (Murray et al. 1995) preventing overionization and likely accounting for X-ray absorption in BAL QSOs (e.g., Gallagher et al. 2006; see also Gibson et al. 2009a and Wu et al. 2010 for discussion of mini-BALs). Observational evidence favoring the disk-wind model includes the relatively high degree of polarization among BAL quasars in general and in BAL troughs in particular (e.g., Ogle et al. 1999; Young et al. 2007; DiPompeo et al. 2011) and the similarity of the spectral energy distributions of BAL and non-BAL quasars (e.g., Willott et al. 2003; Gallagher et al. 2007; but see also DiPompeo et al. 2013). On the other hand, BAL quasars have been argued to accrete at particularly high Eddington ratios (e.g., Ganguly et al. 2007), as inferred based on apparent [O III] weakness (Yuan & Wills 2003). Quasars also possessing low-ionization BALs (LoBALs, in contrast to the more common high-ionization only HiBALs) in particular tend toward weak [O III] and seemingly lack [Ne V] (e.g., Zhang et al. 2010). After accounting for intrinsic absorption, Luo et al. (2013) estimate that 17–40% of BAL quasars are still X-ray weak, and suggest that X-ray weak quasars may more easily launch outflows (due to reduced overionization) with potentially large covering factors.

An initial lack of detected BALs among radio-loud quasars (RLQs) was interpreted to indicate that jets and BALs were mutually exclusive (e.g., Stocke et al. 1992). This paradigm was challenged by a series of discoveries of individual BAL RLQs (e.g., Becker et al. 1997; Brotherton et al. 1998; Wills et al. 1999; Gregg et al. 2000) and then undermined by the identification of a population of BAL RLQs (e.g., Becker et al. 2000, 2001; Menou et al. 2001; Shankar et al. 2008), mostly detected in the VLA 1.4 GHz FIRST survey (Becker et al. 1995) with systematic optical spectroscopic coverage obtained by the FIRST Bright Quasar Survey (FBQS; White et al. 2000) and the Sloan Digital Sky Survey (SDSS; York et al. 2000). Several BAL RLQs display radio spectral and/or morphological properties similar to those of compact steep spectrum (CSS) or GHz-peaked spectrum (GPS) radio sources, which are commonly presumed to be young (e.g., Stawarz et al. 2008), although in general BAL RLQ radio morphologies do not require youth (Bruni et al. 2013). Additionally, dust-reddened quasars (plausibly newly active; Urrutia et al. 2008; Glikman et al. 2012) appear more likely to host low-ionization BALs (Urrutia et al. 2009), suggesting that at least “LoBALs” may be linked to source age rather than inclination. These observations, in concert with the remaining scarcity of BALs within strongly radio-loud and lobe-dominated objects, have revived alternative “evolutionary” models (Gregg et al. 2006) that associate BALs with emerging young quasars clearing their kpc-scale environment through outflows spanning equatorial through polar (e.g., Zhou et al. 2006) latitudes (though a purely evolutionary model requires fine-tuning to match observations; Shankar et al. 2008). The reality may lie between a stark orientation/evolution dichotomy, with some types of quasars more able to host winds that themselves have a range of covering factors (Richards et al. 2011; DiPompeo et al. 2012, 2013). In any event, it is currently unclear whether BALs in RLQs have a similar physical origin to those in RQQs, or indeed whether BALs in RLQs are even a homogeneous class.

Variability studies provide one method of assessing BAL

structure, and they can potentially constrain the location and dynamics of the UV absorber. In principle, BAL variability could be induced through an alteration in the ionization parameter as a result of fluctuations in the incident flux (e.g., Trevese et al. 2013); the variability timescale then constrains the absorber density (Netzer et al. 2002) and/or distance (Narayanan et al. 2004). However, this is unlikely to be the dominant mechanism for cases in which the C IV variability is confined to a restricted velocity segment within the full BAL absorption trough, which indeed constitute the majority of observed variability behavior (e.g., Gibson et al. 2008; Capellupo et al. 2013; see also discussion of saturated C IV outflows in the latter). Alternatively, depth changes within BAL profiles may plausibly arise from dynamical restructuring of the absorber along the line of sight, with the variability timescale providing estimates of crossing speeds and location (Risaliti et al. 2002; Capellupo et al. 2013). Simulations suggest that although the shielding component of the wind can be dynamic (Sim et al. 2012; see also observational X-ray results from Saez et al. 2012), synthesized absorption profiles are relatively constant at lower velocities whereas variability becomes more pronounced at higher velocities, which correspond to well-shielded material streaming to larger distances (Proga et al. 2012). Such disk azimuthal asymmetries can potentially link variability, at differing amplitudes, across multiple velocity components (Filiz Ak et al. 2012). In general, dynamical wind outflow models can produce extremely complex behavior (e.g., Giustini & Proga 2012).

Broad absorption line variability within radio-quiet quasars has now been characterized through several studies, many of which make use of SDSS data for one or more epochs of coverage. BALs in RQQs often show minor depth changes within narrow portions of troughs (Barlow 1993; Lundgren et al. 2007; Gibson et al. 2008, 2010; Capellupo et al. 2011; hereafter B93, L07, G10, and C11, respectively). Variability is perhaps more common within shallower or higher-velocity BALs (L07; C11) which are occasionally even observed to disappear completely (Filiz Ak et al. 2012). BALs of greater equivalent width (EW) tend to show greater absolute changes in EW , and BALs spanning a wider velocity range tend to show variability within a larger absolute subset of velocity bins (Gibson et al. 2008, their Figure 9 and Equation 1, respectively). However, the absolute value of the fractional change in EW is greater in BALs of lower EW (L07), and similarly within a given velocity segment shallower absorption increases the likelihood of variability (C11). Acceleration of BALs is rarely observed (e.g., Hall et al. 2007; Gibson et al. 2008). Changes in velocity width can sometimes transition features out of (or into) formal BAL classification (e.g., Rodríguez Hidalgo et al. 2013; Misawa et al. 2005; see also discussion in Gibson et al. 2009a), indicative of a connection between narrow-absorption line or mini-BAL troughs and the more extreme BALs. While BAL variability is not necessarily monotonic, in general BALs in RQQs tend to vary more often and more strongly on longer timescales (Gibson et al. 2008; G10; C11), although variability on only rest-frame ~ 8 –10 d has been seen (Capellupo et al. 2013).

These results provide a baseline for RQQ BAL variability, but to date there has not been a systematic sur-

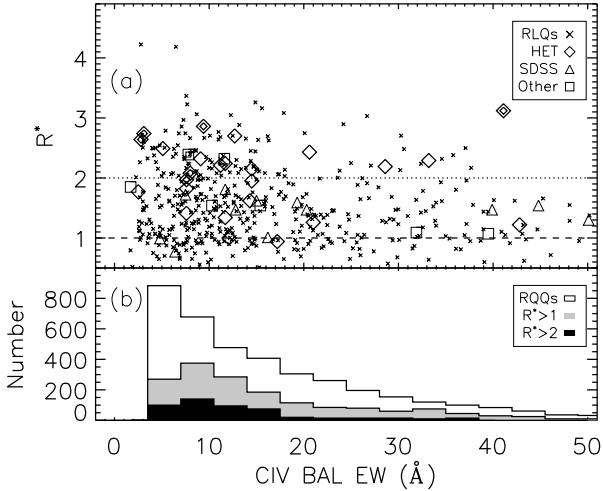


Figure 1. (a) Radio-loudness plotted versus CIV BAL EW. The BAL RLQs studied here from HET/SDSS, SDSS/SDSS, and other archival pairs of spectra are plotted as diamonds, triangles, and squares, respectively. Lobe-dominated RLQs are marked with double symbols. Additional BAL RLQs, identified from the G09 BAL catalog matched to FIRST data, are also shown (crosses). The dashed/dotted lines show increasingly restrictive cuts in R^* . (b) Distribution of CIV BAL EW for RQQs and groups of RLQs.

vey of BAL variability within RLQs² and so no statistical comparison has been possible. This work conducts such a study through measurement of CIV absorption at multiple epochs in a large sample of RLQs. We have obtained 34 new spectra for 28 BAL RLQs, primarily selected as such from FIRST/SDSS data, with the Hobby-Eberly Telescope (HET; Ramsey et al. 1998) Low-Resolution Spectrograph (LRS; Hill et al. 1998). This sample was chosen to cover a wide range in radio-loudness and luminosity and also BAL velocity and equivalent width. BAL variability is assessed through a comparison of the HET/LRS spectra to the earlier SDSS spectra. We also incorporate BAL variability measurements obtained for 18 additional RLQs with two (or more) SDSS or archival spectra available. Together, the 46 RLQs have 78 pairs of BAL equivalent width measurements, probing rest-frame timescales of ~ 80 –6000 d (median 800 d).

This paper is organized as follows: §2 describes the selection and radio and BAL characteristics of the sample, §3 quantifies BAL variability, §4 compares to results for BAL RQQs and investigates dependencies upon continuum variability and radio properties, and §5 summarizes and concludes. We use positive values of equivalent width (given in units of rest-frame Å) to quantify BAL absorption strength, and express changes in equivalent width such that a positive difference corresponds to the BAL deepening between observations. A standard cosmology with $H_0 = 70 \text{ km s}^{-1} \text{ Mpc}^{-1}$, $\Omega_M = 0.3$, and $\Omega_\Lambda = 0.7$ is assumed throughout. Monochromatic luminosities are given in units of $\text{erg s}^{-1} \text{ Hz}^{-1}$ and expressed as logarithms, with ℓ_r and ℓ_{uv} determined at rest-frame 5 GHz and 2500 Å, respectively. Unless otherwise

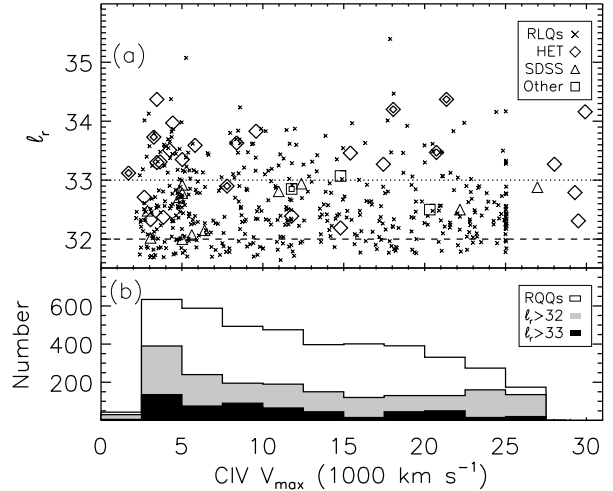


Figure 2. (a) Radio luminosity plotted versus CIV maximum outflow velocity, with symbols as in Figure 1. Note that the maximum outflow velocity is restricted to 25000 km s^{-1} in G09. The dashed/dotted lines show increasingly restrictive cuts in ℓ_r . (b) Distribution of v_{max} for RQQs and for RLQs with cuts as above.

noted, errors are quoted at 1σ . Object names are given as SDSS J2000 and taken from the DR7 Quasar Catalog of Schneider et al. (2010; see also Schneider et al. 2005, 2007).

2 SAMPLE CHARACTERISTICS

General optical, radio, and (longest separation) absorption properties of the 46 BAL RLQs studied here are listed in Table 1. We restrict consideration of absorption variability to the CIV line. The sample consists primarily of HiBALs; only 5/46 RLQs are known LoBALs (although for RLQs with $z > 2.1$ the Mg II line is redshifted out of SDSS coverage). The objects consequently have redshifts $1.7 < z < 4$ so as to be accessible to ground-based telescopes, except for 100726.10+124856.2 (PG 1004+130; $z = 0.241$) which has *IUE* and *HST* coverage.

2.1 Sample selection

The 28 objects observed with the HET were identified as BAL quasars in the SDSS DR3 catalog of Trump et al. (2006) and the SDSS DR5 catalog of Gibson et al. (2009b; hereafter G09). (The one exception to the HET targeting of SDSS quasars is 101614.26+520915.7, discovered and described in Gregg et al. 2000, which we include to increase the size of our subsample of lobe-dominated BAL RLQs.) One of the 28 HET targets is listed in Trump et al. (2006) but not also identified as a BAL quasar in Gibson et al. (2009b): J074610.50+230710.7 has two deep adjacent absorption troughs (in both CIV and SiIV), which if considered together reach BAL width ($> 2000 \text{ km s}^{-1}$). RLQs (defined as in §2.2) were identified through cross-matching to the FIRST survey catalog, with all radio components within $90''$ initially retained and then visually classified as either lobes (e.g., an approximately symmetric pair about the optical source) or else as background (e.g., with an SDSS counterpart, or an unrelated intruding double). HET targets were

² A preliminary sketch of some portions of this paper is given in Miller et al. (2012). Filiz Ak et al. (2013) study BAL quasars in SDSS and briefly compare RQQs to a small set of RLQs.

selected to have $1.7 < z < 4.0$ to permit optical access to the C IV region. The HET targets span a wide range in radio and BAL properties, and as demonstrated in §2.2 our full sample is representative of the parent population of BAL RLQs with respect to BAL equivalent width or maximum velocity, and with respect to radio luminosity or radio loudness. For feasibility purposes brighter targets were preferred, and as the redshift coverage is representative this results in the SDSS/HET objects having somewhat greater optical luminosities than the parent population of BAL RLQs.

An additional 18 BAL RLQs with multiple SDSS or archival spectra are included in our full sample. Most of these objects were identified as BAL RLQs through cross-matching the G09 catalog with FIRST as for the HET sample. The separation between spectra was required to exceed rest-frame 15 d. The SDSS/SDSS objects are observed on relatively short rest-frame timescales, similar to the 20–120 d range probed by the multi-epoch SDSS study of BAL RQs conducted by Lundgren et al. (2007). A few of the SDSS/HET objects also have multiple SDSS spectra, and we also quantify their shorter timescale variability. A handful of these additional BAL RLQs were selected from the literature (e.g., L07; G10; C11), including 100726.10+124856.2 (PG 1004+130), identified as a BAL RLQ and described in Wills et al. (1999), for which we here add a previously unpublished *HST* spectrum to archival *IUE* coverage.

2.2 Radio and optical properties

The radio and optical properties of the BAL RLQs studied here are given in Table 1. We use radio and optical/UV monochromatic luminosities with units of $\text{erg s}^{-1} \text{Hz}^{-1}$ at rest-frame 5 GHz and 2500 Å, and ℓ_r and ℓ_{uv} are expressed as logarithms. Radio-loudness is taken to be the logarithmic ratio of monochromatic luminosities measured at (rest-frame) 5 GHz and 2500 Å (e.g., Stocke et al. 1992; c.f. Kellerman et al. 1998), so $R^* = \ell_r - \ell_{uv}$. The optical/UV luminosity is calculated at rest-frame 2500 Å using SDSS photometry [specifically, the nearest one or two magnitudes to $2500(1+z)$ Å, corrected for Galactic extinction] through comparison to a redshifted composite quasar spectrum (Vanden Berk et al. 2001) convolved with *ugriz* filters. The radio luminosity is calculated at rest-frame 5 GHz using catalog FIRST peak fluxes for the core, and integrated fluxes for the lobes, assuming typical radio spectral indices of $\alpha = -0.3/\alpha = -0.9$ for core/lobe components.

Figure 1 shows C IV EW versus R^* for our sample in the top panel, along with values for other BAL RLQs (also identified through matching to FIRST data). A histogram of EW values (from G09) for BAL RLQs and for BAL RQs is provided in the lower panel. As previously noted (see §1), there is a paucity of objects that are simultaneously strongly radio loud and heavily absorbed. However, our sample includes objects spanning the full range of R^* and EW that are typical of BAL RLQs, and its distribution is representative of that class.³ Figure 2 shows C IV v_{max} versus ℓ_r for

³ Kolmogorov-Smirnov (KS) tests comparing EW give probability $p = 0.17$, indicating the distributions are not inconsistent; similarly, for R^* we find $p = 0.19$. BAL RLQs and BAL RQs have formally inconsistent distributions of EW ($p = 0.006$).

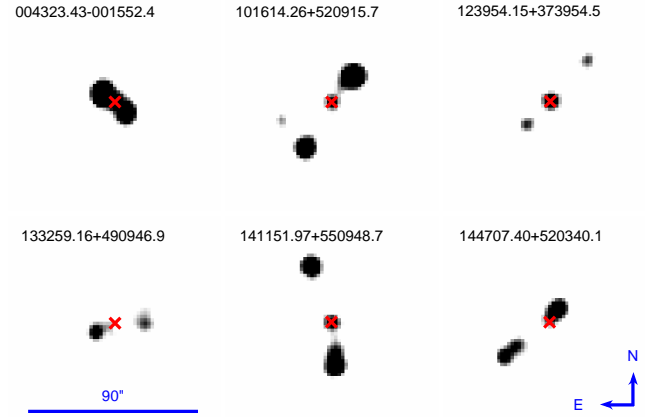


Figure 3. FIRST 1.4 GHz radio maps of the lobe-dominated BAL RLQs for which we obtained new HET spectra. The angular resolution is $\simeq 5''$. The SDSS position of the quasar core is marked with a cross. The flux density is plotted on a consistent logarithmic scale.

our sample in the top panel, again with values for other BAL RLQs, with a histogram of v_{max} provided in the lower panel (from G09; note they truncate BALs beyond 25000 km s^{-1}). Here too our sample spans the full range of parameter space and is representative of BAL RLQs in general.⁴

Radio maps of the six lobe-dominated BAL RLQs for which we obtained new HET spectra are provided in Figure 3, from the 1.4 GHz FIRST survey, with the optical SDSS position indicated with a red cross. The radio morphology of PG 1004+130 is shown and discussed in Gopal-Krishna & Wiita (2000) and Miller et al. (2006).

3 BAL VARIABILITY IN RLQS

Our measurements of C IV absorption equivalent widths for each absorption trough, in each object, at each epoch, are listed in Table 2. The associated variability measures (change in equivalent width, ΔEW , and absolute fractional change, $|\Delta EW|/\langle EW \rangle$), for each pair of spectra are given in Table 3. Examples of data reduction and analysis are given in Figures 4, 5, and 6; all spectra are provided in Appendix A. Spectral variability in a few individual objects of interest is highlighted in Figures 7, 8, and 9.

3.1 Observations and data reduction

The HET observations were obtained in queue-scheduled mode in 2007–2008 and 2011 (see Table 2). The LRS was used for the spectroscopic observations, in almost all cases with the g2 grating and typically with a $1.5''$ slit. This configuration provides a spectral resolution of $R \simeq 870$ (or $\sim 340 \text{ km s}^{-1}$ at observed 5500Å), which is sufficiently closely matched to that of SDSS (typical resolution $R \simeq 1800$, or 170 km s^{-1}) to permit effective evaluation of BAL variability. The HET data were reduced in standard fashion

⁴ KS tests comparing v_{max} give probability $p = 0.44$, indicating the distributions are not inconsistent; similarly, for ℓ_r we find $p = 0.16$ when restricting to $\ell_r > 32$.

using the Image Reduction and Analysis Facility (IRAF⁵). In brief, we generated and subtracted a master bias, using a 30×800 overscan stripe to account for time-dependent changes; created a normalized master flat from internal lamp frames, and divided this into the object frames to remove pixel-to-pixel sensitivity variation; subtracted the sky background using apertures of 100 pixel width offset by 50 pixels from the object (shifted if necessary to avoid background objects); manually identified and interpolated over cosmic rays; traced the aperture and extracted a one-dimensional spectrum; applied wavelength calibration based on ThAr comparison spectra; shifted wavelengths to the heliocentric frame; applied relative flux-calibration based on a standard star (absolute flux calibration is not required, as we use normalized spectra — this step is primarily useful to remove the blaze function).

The SDSS spectra were downloaded⁶ and wavelengths were converted to air values for direct comparison to our HET spectra. For both HET and SDSS or other archival data, we modeled the continuum with a low-order (second or third) Chebyshev polynomial, masking the $L\alpha$ and NV , $Si\ IV$, and $C\ IV$ emission line regions as well as any obvious BAL absorption, and additionally imposing strict multi-pass σ rejection criteria to bypass less prominent lines or weak BALs. The resulting best-fit continuum polynomial was then divided out to normalize the spectra near the $C\ IV$ region. This implicitly dereddens the spectra. Typically the same polynomial constraints (wavelength ranges for fitting, polynomial order) were used to normalize all spectra for a given object.

3.2 Measurement of absorption properties

Wavelengths are converted to the rest-frame of the quasar using the improved redshifts calculated from SDSS spectra by Hewett & Wild (2010) where available, or else from other sources including the NASA/IPAC Extragalactic Database.⁷ We restrict our focus to BAL variability, and so any emission-line variability or remaining residual continuum variability is modeled out. We fit a Voigt profile to the $C\ IV$ emission line in each spectrum (including a linear residual continuum term), choosing this model for convenience in matching observations but ascribing no particular physical significance to the functional form (see also, e.g., G10). The emission-line parameters are calculated for the highest signal-to-noise observation and then applied to the other observations; for a few cases in which the emission profile has obviously varied, the lower signal-to-noise observations are fit independently. The continuum placement and slope is always permitted to vary. In cases for which the BAL absorption extends within the emission-line region, it often proved necessary to adjust manually the fit parameters to obtain a satisfactory model. Similar fitting to an empirical RLQ spectral template from Kimball et al. (2011) provided the initial parameters for the $C\ IV$ emission line profile, and was adhered to as closely as possible where absorption prevented automated fitting. To simplify analysis

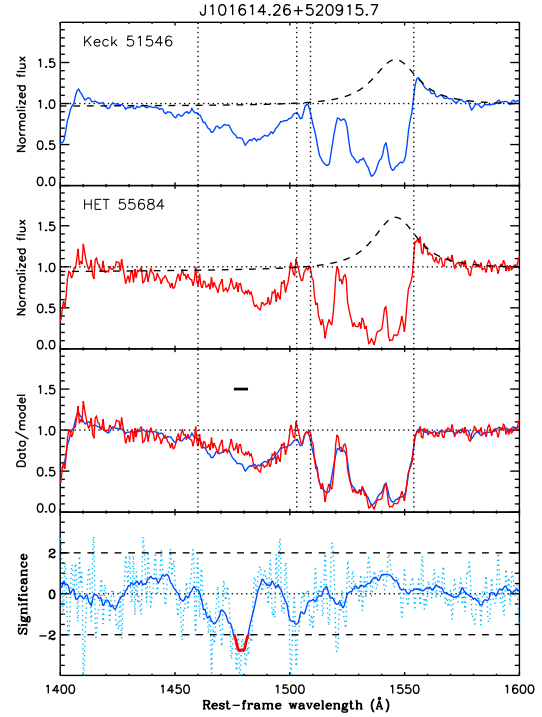


Figure 4. Illustration of measurement of BAL properties. The $C\ IV$ emission line is modeled with a Voigt profile (dashed lines, top two panels) and divided out, then the equivalent width is calculated within the BAL region (vertical dotted lines). In this case the BAL varied significantly at $1476\text{--}1482\ \text{\AA}$ (bottom panel) between the two observations. Variability in the bottom panel is plotted in units of σ (dotted cyan line) as the difference between the normalized spectra divided by the typical uncertainty (as measured empirically in a non-varying flat region of the continuum), then smoothed (solid blue line) prior to checking for any $> 2\sigma$ changes (solid red line overplotted, where present).

of the absorption properties, the $C\ IV$ emission-line model is then divided out, and BAL properties are measured from the resulting ratio spectrum.

The edges of a BAL are here defined to be the wavelengths at which the BAL intersects 90% of the normalized continuum, following Weymann et al. (1991). An example is shown in Figure 4. The only exception occurs for J123411.74+615832.5, for which the HET spectrum does not fully cover the BAL; here the maximum considered velocity is fixed to the limit of high S/N HET coverage. BALs are required to have velocity widths $\gtrsim 2000\ \text{km s}^{-1}$, but are allowed to be present at velocities ranging from zero (or even slightly redshifted) to $30000\ \text{km s}^{-1}$, beyond the classical 3000 to $25000\ \text{km s}^{-1}$ boundaries often imposed (e.g., Weymann et al. 1991; G09). The equivalent width of each $C\ IV$ BAL is then calculated as a sum over all pixels within the BAL region (recall all artifacts have been removed). The error on the equivalent width is calculated including contributions from three sources: fitting error in the continuum placement, statistical noise in the spectrum (which may be higher within the BAL region), and measurement uncertainty in the BAL edge determination. The first term is estimated as the standard deviation of the data within a flat $50\ \text{\AA}$ region, and is applied pixel-by-pixel. The next term is estimated as the deviation from a smoothed

⁵ <http://iraf.noao.edu/iraf/web/>

⁶ <http://www.sdss.org>

⁷ <http://ned.ipac.caltech.edu/>

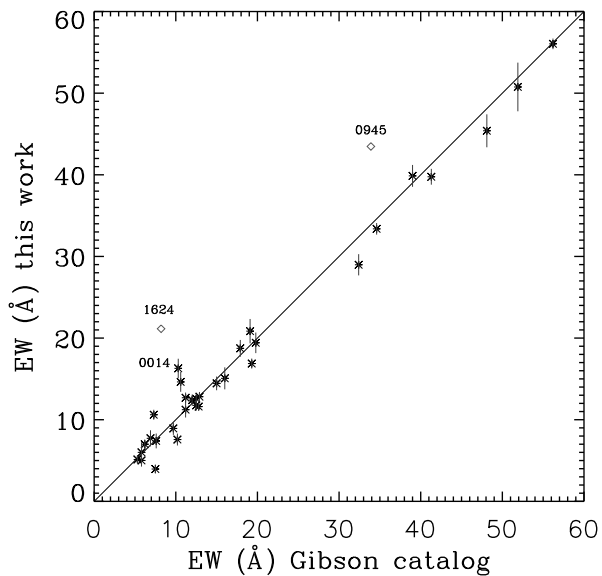


Figure 5. Our equivalent width measurements for BAL RLQs compared with those determined by G09 for the same SDSS quasars. There is close agreement; the mean difference is 0.12 \AA . The open diamonds mark objects for which the full BAL extends beyond the 25000 km s^{-1} boundary considered in G09. Typical 1σ statistical errors on the G09 measurements are $\pm 1 \text{ \AA}$.

spectrum at each point; it is added in quadrature to the first term. The final term is estimated by recalculating the equivalent width using BAL edges shifted by $\pm 0.5 \text{ \AA}$; the absolute value of the difference is added in quadrature to the sum of the first and second terms. Our equivalent width measurements agree well with those conducted by Gibson et al. (2009b) for the SDSS quasars (at a given epoch) in common (Figure 5). After removing two objects with BALs extending beyond the 25000 km s^{-1} boundary considered by Gibson et al. (2009b), the mean difference is only 0.12 \AA . The largest remaining outlier is an object for which G09 exclude a low-velocity component which our continuum/emission fit includes in the primary BAL.

The time interval between spectra in the quasar rest frame is determined as $\tau = (MJD_{\text{new}} - MJD_{\text{old}})/(1+z)$, where the modified Julian dates correspond to the midpoints of the respective observations. The average equivalent width for a given object is simply $\langle EW \rangle = 0.5(EW_{\text{new}} + EW_{\text{old}})$, and the change in equivalent width is $\Delta EW = EW_{\text{new}} - EW_{\text{old}}$, so that a positive value of ΔEW signifies an increase in EW (e.g., a BAL becoming deeper). The absolute fractional change in equivalent width is $|\Delta EW|/\langle EW \rangle$.

Potential velocity shifts within the BAL structure were assessed through shifting one spectrum relative to the other and minimizing the squared residual (Hall et al. 2007). An example is shown in Figure 6. No significant examples of bulk velocity shifts in BAL features were found, with limits typically around $\lesssim 100 \text{ km s}^{-1}$. For the longest rest-frame timescales within our sample of $\sim 1000 \text{ d}$, this limits average acceleration to $\lesssim 0.1 \text{ cm s}^{-2}$.

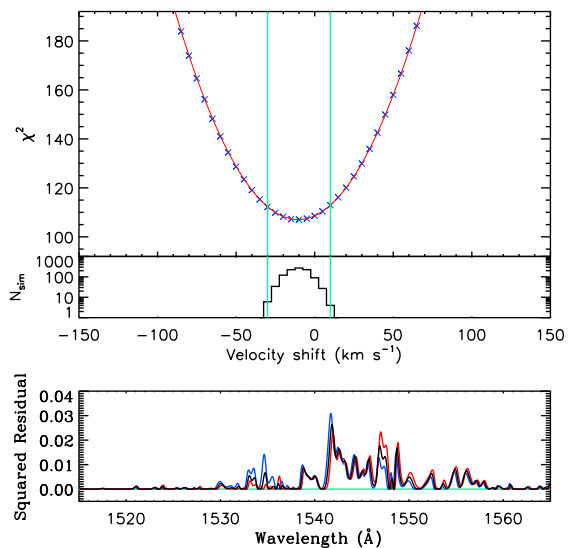


Figure 6. Illustration of assessment of velocity shifts between epochs. One spectrum is shifted relative to the other to identify the optimal wavelength offset (lowest squared residual; bottom); in this case, the 99% confidence region includes zero (top). Simulations confirm that the errors are consistent (middle).

3.3 Notes on individual objects

Here we describe individual objects of interest within our sample of BAL RLQs. For additional notes on some objects, see also §3.3 of Miller et al. (2009).

Known LoBAL quasars: Four of these BAL RLQs have absorption at ions other than C IV or Si IV in the SDSS catalog of G09: J083925.61+045420.2 and J132139.86−004151.9 have Al III absorption and lack SDSS Mg II coverage, while J094513.89+505521.8 and J123954.15+373954.5 have both Al III and Mg II absorption. J141546.24+112943.4 is in DR6+ but not DR5 so it is not included in G09, but inspection of the SDSS spectrum shows Al III absorption, previously identified as broad by Hazard et al. (1984). Note that for the BAL RLQs with $z > 2.1$ the Mg II line is redshifted beyond SDSS coverage.

Mini-BAL absorption: In addition to its high-velocity BAL, J162453.47+375806.6 also has lower-velocity absorption described by Benn et al. (2005) as a mini-BAL. Some of the narrower BALs studied here are elsewhere (e.g., Rodriguez Hidalgo et al. 2012) considered as mini-BALs, including J115944.82+011206.9.

Lobe-dominated RLQs: Seven of the BAL RLQs studied here have radio emission dominated by bright radio lobes (Figure 3). J004323.43−001552.4 (Gregg et al. 2006; Brotherton et al. 2006, 2011), J133259.16+490946.9, and J144707.40+520340.1 (Gregg et al. 2006) are all included in the catalog of SDSS FR II quasars of de Vries et al. (2006), while J100726.10+124856.2 (Wills et al. 1999) and J101614.26+520915.7 (Gregg et al. 2000) were among the first-identified BAL RLQs. J123954.15+373954.5 and J141151.97+550948.7 are also lobe-dominated. These objects are presumably viewed at relatively large inclinations (e.g., Wills & Brotherton 1995).

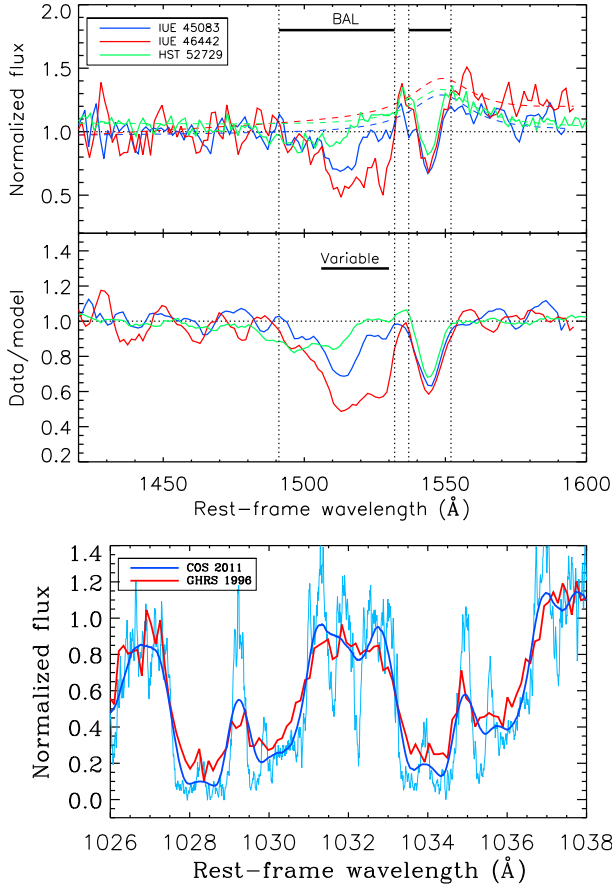


Figure 7. PG 1004+130 BAL absorption variability. Top, upper: observed C IV spectrum with continuum and emission line model shown. Top, lower: normalized spectrum boxcar smoothed by 5 pixels (6.8 Å). Note the increase and subsequent decrease in absorption depth within a segment of the high-velocity outflow component over 16.9 rest-frame years. Bottom: O VI low-velocity absorption with COS (cyan) and GHRS (red); when the COS resolution is degraded (blue) with a Gaussian kernel to match the GHRS spectrum, only slight changes in the depths of the troughs are found, in contrast to the dramatic C IV variability.

Small-scale structure: Several of the core-dominated RLQs display one-sided jet emission on mas scales, including J115944.82+011206.9 (here a short counterjet feature is also present near the core; Montenegro-Montes et al. 2009), J141334.38+421201.7 (Liu et al. 2008), and J162453.47+375806.6 (Benn et al. 2005, Montenegro-Montes et al. 2009).

Flat radio spectrum: Several RLQs have 5 GHz Green Bank data (or low-frequency observations) that suggest they have flat ($\alpha \gtrsim -0.3$) radio spectra, including J074610.50+230710.7, J085641.56+424253.9, J105416.51+512326.0, J133701.39−024630.2, and J141334.38+421201.7. A flat radio spectrum in a core-dominated RLQ indicates a relatively low inclination. The radio spectrum of J115944.82+011206.9 is double-peaked (Montenegro-Montes et al. 2009) so this may be a younger source.

J100726.10+124856.2: This low-redshift lobe-dominated BAL RLQ (PG 1004+130, $z = 0.241$,

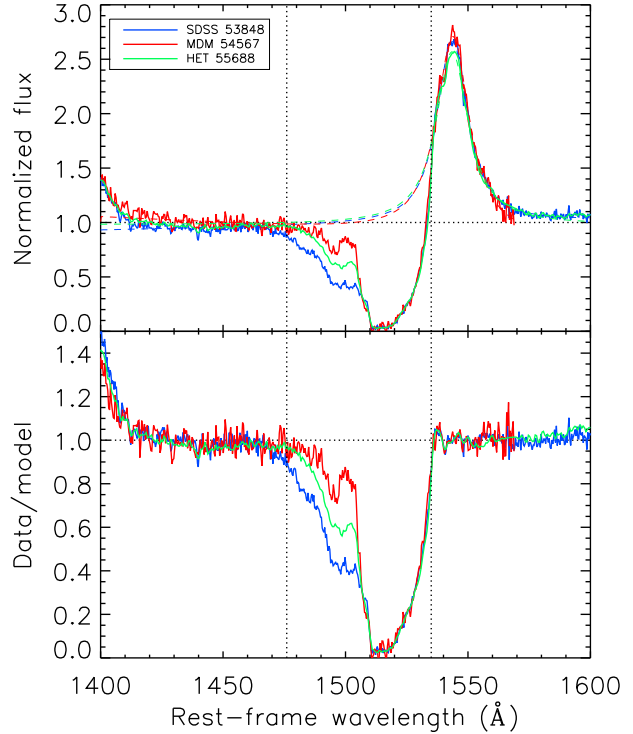


Figure 8. J141546.24+112943.4 spectra from SDSS, MDM, and HET, showing a strong decrease in absorption strength followed by a partial recovery toward increased absorption. See also C11.

$M_B = -25.6$; Wills et al. 1999; Brandt et al. 2000) is known to show variable X-ray absorption (Miller et al. 2006). Here we show that it also possesses strongly variable C IV absorption (Figure 7), for example with the primary BAL greatly diminishing in depth from the January 1986 IUE observation to the March 2003 HST/STIS spectrum (~ 14 rest-frame years). PG 1004+130 displays the greatest absolute and fractional equivalent-width variations in our survey of BAL RLQs. The lower-velocity absorption is also seen at higher ionizations, including OVI. A comparison of the OVI absorption from recent FUV COS/G130M observations with a GHRS spectrum from 1996 shows perhaps a slight increase in the depths of the troughs (Figure 7), but this modest variability is of substantially lower amplitude than is seen in the primary C IV BAL at higher velocities. The slower interior flow is more exposed to direct high-energy radiation⁸ and is consequently more highly ionized; the OVI doublets are optically thick and partially covering (Wills et al. 1999).

141546.24+112943.4: This is the extensively studied “cloverleaf” quasar H1413+117, a gravitationally lensed object that is split into 4 images separated by $\sim 1''$. The A image shows enhanced X-ray emission, suggestive of microlensing (Chartas et al. 2004), and based on CO emission the quasar is surrounded by a rotating molecular disk (Venturini

⁸ In BAL RLQs, this may include a small-scale jet contribution (e.g., Miller et al. 2009).

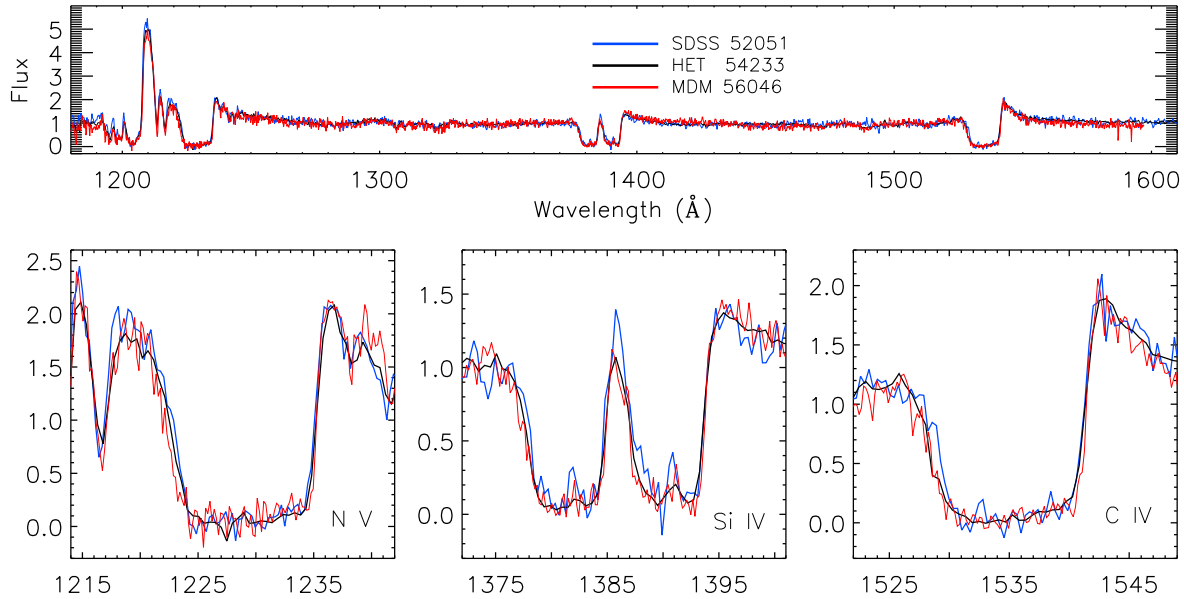


Figure 9. SDSS, HET, and MDM spectra of the BAL RLQ J160943.35+522550.8 (top), with details of the C IV, Si IV, and NV absorption regions (bottom). The BALs in the HET spectrum (black) extend to slightly greater velocities than in the earlier SDSS spectrum (blue), but align with the later MDM spectrum (red). This illustrates that an apparent acceleration between two epochs might instead result from a change in depth within a high-velocity segment, here identifiable in the third epoch data.

& Solomon 2003). This modestly radio-loud ($R^* = 1.09$) quasar displays variability within the higher-velocity half of the primary BAL while the lower-velocity segment remains constant. Between the SDSS and subsequent MDM spectra (MDM data from C11, see that work for details), the absorption decreases in strength, but by the latest HET spectrum the absorption is again increasing in strength (Figure 8). As noted above, this is one of the few known LoBALs in our sample.

J160943.35+522550.8: This object showed an apparent increase in the maximum velocity of the BAL outflow between the SDSS and HET observations. While the red edge remained fixed, the blue edge extends to shorter wavelengths in the later HET data, in not only C IV but also Si IV and NV (Figure 9). Systematic changes in the velocity structure of a BAL are unusual, for either BAL RQQs or BAL RLQs (e.g., Hall et al. 2007; Gibson et al. 2008). We obtained a new MDM spectrum to check whether a high-velocity component had accelerated between epochs, leaving the main absorption trough unchanged due to the putative presence of additional absorbers partially overlapping in velocity space and together fully covering the continuum. The MDM observations were carried out using the 2.4m Hiltner telescope with the Ohio State Multi-Object Spectrograph (VPH grism, center 1.2'' slit). The MDM spectrum aligns with the HET spectrum (Figure 9), arguing against acceleration and suggesting instead that a high-velocity component was always present but increased in strength (e.g., through a highly ionized clump cooling to a greater C IV opacity), or that a high-velocity cloud transversely entered the line of sight. This illustrates the importance of obtaining a third epoch spectrum to check cases of potential acceleration.

4 ANALYSIS AND DISCUSSION

Below, we investigate the distributions of absolute change in equivalent width $|\Delta EW|$ and absolute fractional change in equivalent width $|\Delta EW|/\langle EW \rangle$ as a function of rest-frame interval between spectral observations ($\Delta\tau$; Figure 10) and of average BAL equivalent width ($\langle EW \rangle$; Figure 11). Variability is also assessed with respect to velocity width (Figure 12), and comparisons are made to BAL variability patterns within RQQs. Optical continuum variability is assessed and quantified for BAL RLQs (Figure 13) and BAL RQQs (Appendix B, Figures 1 and 2) and compared across classes (Figures 14 and 15). For RLQs, the impact of radio loudness or luminosity (R^* or ℓ_r) upon BAL variability is investigated (Figure 16). The longest-separation total BAL absorption properties for BAL RLQs and for the comparison sample of BAL RQQs are given in Tables 1 and 4, respectively.

For a portion of the analysis it is convenient to distinguish between subsamples of BAL RLQs grouped by radio properties. RLQs are separated into core-dominated or lobe-dominated, low or high radio luminosity (at $\ell_r = 33$), and low or high radio loudness (at $R^* = 2$). Note that while the archival coverage of PG 1004+130 (lobe-dominated, low radio luminosity, high radio loudness) extends to longer timescales than are typical within our sample, for this object the variability over ~ 1000 d is actually larger than for the longest separation ~ 6000 d measurement used.

Median and mean properties, along with Kolmogorov-Smirnov (KS) test probabilities for selected comparisons, are provided in Table 5. Correlation likelihoods (non-parametric Kendall τ and Spearman ρ) and coefficients along with best-fit linear regression slopes and errors (calculated using the IDL `robust_linefit` routine) for each tested relationship are listed in Table 6.

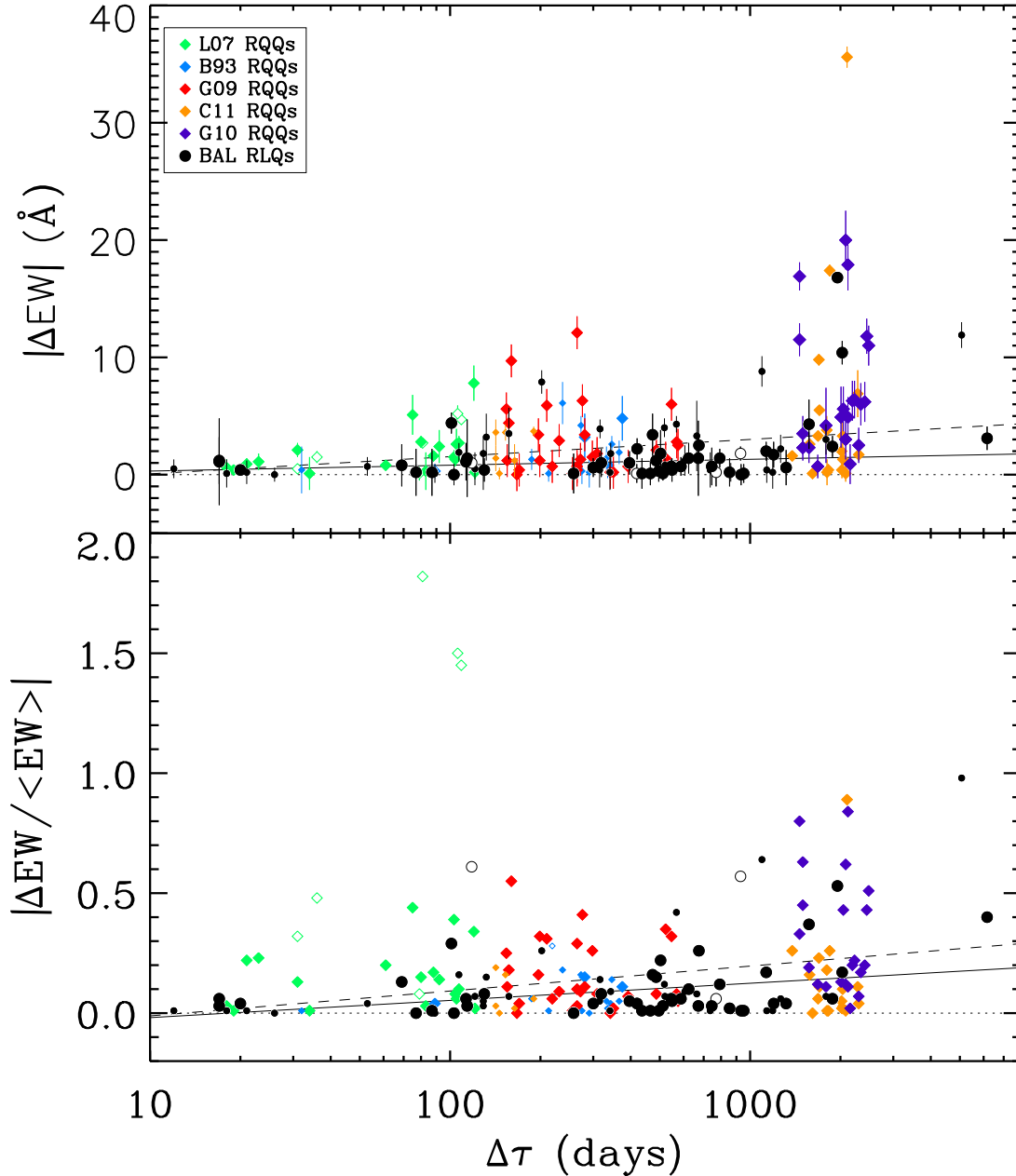


Figure 10. Change in BAL equivalent width and absolute fractional change in BAL equivalent width versus interval between spectroscopic observations for RQQs (diamonds) and RLQs (circles). RQQ subsamples plotted in green/blue/red/orange/purple are from L07/B93/G09/C11/G10, respectively, and open symbols have $EW < 3.5$ Å. For objects with multiple pairs the shorter-separation measurements are plotted using smaller markers. The dashed and solid lines show linear fits to RQQs and RLQs; the dotted line is zero.

4.1 Comparison to BAL RQQs

To avoid potential biases arising from repeated sampling of particular objects (recall we have 78 pairs of spectra of 46 BAL RLQs), the longest-separation measurement of variability available for each of the 46 BAL RLQs is used for all statistical comparisons to RQQs. We constructed a comparison sample of BAL RQQs from previous studies of BAL variability (B93, L07, G09, G10, and C11), for verified radio-

quiet⁹ quasars; recall from §2.1 that the handful of RLQs covered in these studies are included in our radio-loud sample. In particular, we use 25 pairs of spectra from dual-epoch

⁹ We checked radio-loudness against FIRST data where possible, otherwise against the NASA/IPAC Extragalactic Database (NED; <http://ned.ipac.caltech.edu/>); note that the RQQs LBQS 0055+0025 and [HB89] 2225–055 are near unassociated radio sources.

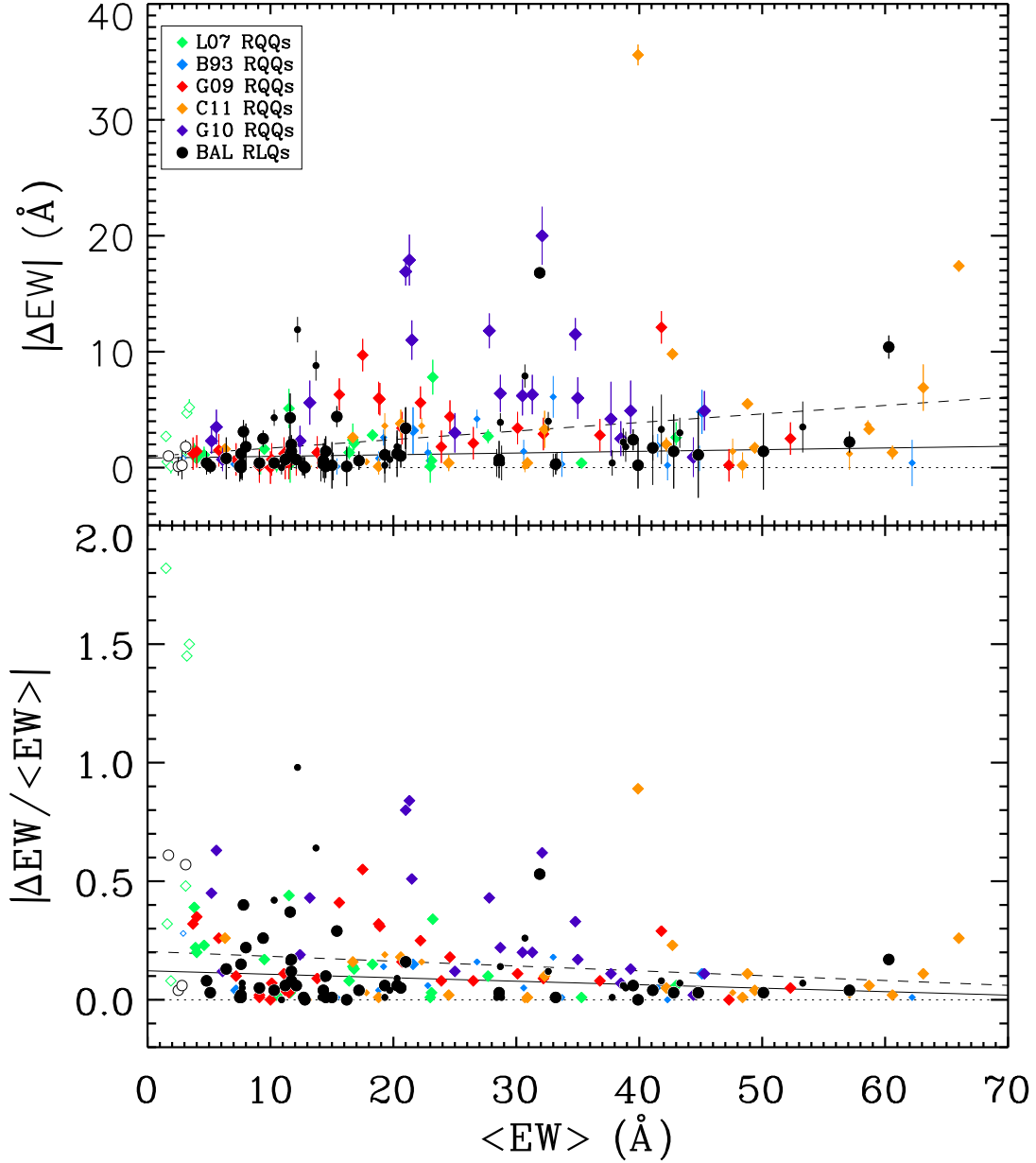


Figure 11. Change in BAL equivalent width versus average BAL equivalent width for RQQs (diamonds) and RLQs (circles). Symbols as in Figure 10. There is a tendency ($\geq 95\%$ confidence) toward greater $|\Delta EW|$ within stronger BALs, for both RLQs and RQQs.

SDSS measurements from L07 and another 28 from G09 (requiring $\Delta\tau > 150$ d, hence distinct from L07); 16 pairs of spectra from dual-epoch Lick measurements from B93 (some additional measurements from this reference are superseded by C11); 21 pairs of spectra from Lick/SDSS/HET spectra from G10; and 25 pairs of spectra from Lick/SDSS/MDM spectra from C11. Together, these studies cover short (20–120 d; L07), short/intermediate (80–400 d; B93), intermediate (130–600 d; G09), intermediate/long (100–200 d and 1300–3000 d; C11), and long (1300–2500 d; G10) timescales. The combined sample of RQQs then includes 115 pairs of BAL absorption measurements. From these, we construct

a longest-separation sample with a single measurement of BAL variability for each of the 94 unique BAL RQQs.

Four RLQs and six RQQs have small absorption equivalent widths $\langle EW \rangle < 3.5$ Å which are not typical of BALs; following Gibson et al. (2008), we compare RQQs and RLQs after removal of these objects. The resulting filtered longest-separation samples of 42 RLQs and 88 RQQs with $\langle EW \rangle \geq 3.5$ Å span similar ranges in redshift and luminosity, but have inconsistent distributions (KS test $p < 0.03$ of being drawn from the same underlying population) of both $\Delta\tau$ and $\langle EW \rangle$, in the sense that these RQQs cover longer timescales and have larger BAL equivalent widths.

We constructed a matched group of 42 RQQs through selecting objects with $\Delta\tau$ and $\langle EW \rangle$ values similar to those of the filtered RLQs, without consideration of any variability properties (the KS probabilities for the matched RQQ sample are now $p = 0.26$ and $p = 0.56$ for $\Delta\tau$ and $\langle EW \rangle$, respectively). The filtered samples of 42 RLQs and 88 RQQs were also divided into groups of short and long timescale (at $\Delta\tau = 500$ d, which is approximately the median timescale for both samples) and moderate and large average equivalent width (at $\langle EW \rangle = 20$ Å, which is approximately the median equivalent width for the BAL RQQs).

In general, BAL variability within RLQs appears similar to that within RQQs. Qualitatively, variability within RLQs, when observable, typically consists of a modest change in the absorption depth, often within a discrete section of the full trough (Figures 4, 7, 8, and Appendix A). Velocity shifts in the structure of BALs appear to be rare (one candidate from our 46 BAL RLQs; Figure 9). These are similar to established tendencies within BAL RQQs (§1). Quantitatively, prior to filtering or matching, the absolute change in EW or fractional variability is lower within RLQs (e.g., the mean $|\Delta EW|/\langle EW \rangle$ is 0.12 ± 0.02 for RLQs versus 0.24 ± 0.03 for RQQs). After filtering out objects with $\langle EW \rangle < 3.5$ Å, the fractional variability in RLQs is still smaller (0.10 ± 0.02 versus 0.19 ± 0.02), and this difference persists in the matched RQQs (0.17 ± 0.03 ; this is a $\sim 2\sigma$ difference); the KS test probability of $p = 0.01$ is likewise marginally inconsistent with RLQs and matched RQQs possessing similar BAL variability. The percentage of RLQs displaying significant BAL variability is $21\% \pm 7\%$ (Poisson errors; Table 3 and Appendix A), lower than is typical for BAL RQQs on similar timescales (e.g., C11).

It is possible that this comparison could be influenced by systematic differences in how BAL variability is measured across different studies; for example, our approach of locking continuum and emission line fit parameters as well as BAL edges between epochs wherever possible may produce lower changes in EW than would result from completely independent fitting and measurement at each epoch. An additional point of concern is that our identification of variability is sensitive to noise. There is an apparent anti-correlation between BAL variability and optical magnitude (at $\sim 2\sigma$ significance) for the combined RLQ and RQQ sample. However, the optical magnitudes of the RLQs are similar to those of the matched RQQs (KS test probability $p = 0.54$), with means of 18.46 ± 0.14 and 18.34 ± 0.10 , respectively. We conservatively interpret our results to indicate that BAL RLQs show similar or perhaps decreased BAL variability as compared to BAL RQQs. This is consistent with the findings of Filiz Ak et al. (2013) of no significant differences in variability, for a smaller sample of BAL RLQs.

BALs in RLQs are more likely to vary and display a greater variability amplitude on longer timescales (Figure 10), similar to established trends for BAL RQQs (§1). The mean $|\Delta EW|/\langle EW \rangle$ is 0.13 ± 0.03 (0.06 ± 0.02) for $\Delta\tau \geq 500$ d (< 500 d). The corresponding mean values for a matched sample of BAL RQQs are somewhat greater (0.23 ± 0.04 and 0.15 ± 0.02 , respectively), although within the longer timescale bin the full distributions of $|\Delta EW|/\langle EW \rangle$ are not inconsistent. Kendall and Spearman tests also find a significant if only moderately strong correlation between $\Delta\tau$ and $|\Delta EW|$ (Table 6) for both RLQs

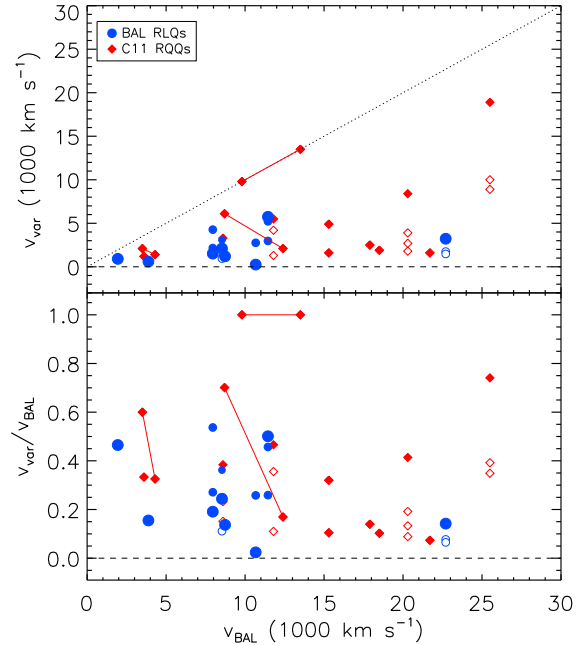


Figure 12. Illustration of velocity width over which BALs varied for RLQs (blue circles) and RQQs from C11 (red diamonds). The open symbols are the sub-sections of a given trough that varied. For the RQQs, 3 objects have variability within two distinct troughs (connected with lines). For RQQs we only plot the longest separation measurements for clarity. For the RLQs, the longest separation measurement is plotted as larger symbols, the shorter epoch(s) as smaller symbols.

and RQQs. The best-fit slope for $|\Delta EW|$ as a function of $\log \Delta\tau$ is greater for RQQs. Both BAL RLQs and BAL RQQs also tend to have larger absolute (but not fractional) changes in equivalent width within stronger BALs (Figure 11). The mean ΔEW for RLQs is 3.2 ± 1.2 Å (1.1 ± 0.2 Å) for $\langle EW \rangle \geq 20$ Å (< 20 Å). Correlation tests again provide agreement in identifying a significant if moderate trend for both RLQs and RQQs, again with larger best-fit slopes for RQQs. Note that the mean and median timescales are similar in the two groupings of RLQs split by average BAL equivalent width, so we can be confident that this is a distinct trend from the correlation with timescale (the average equivalent widths are also similar between the RLQ groups split by timescale). This is not the case for the RQQs, so here the RLQs provide a cleaner demonstration of the trends (previously discovered in RQQs; see §1) toward increasing BAL variability on longer timescales or (in an absolute but not fractional sense) within stronger BALs.

BALs in RLQs tend to vary within only a fraction of the full velocity width of the BAL trough, similar to RQQs (Gibson et al. 2008; G10; C11). We define v_{BAL} to be the velocity span calculated from the wavelength edges of the BAL, as defined in §3.2 and listed in Table 3, and v_{var} to be the velocity span of the variable portion within the BAL. Figure 12 plots the velocity widths v_{var} and $v_{\text{var}}/v_{\text{BAL}}$ against v_{BAL} , for those RLQs with significant BAL variability and for RQQs from C11. Here the open symbols show the segments of a given trough that varied (three RQQs with variability within two distinct troughs are connected

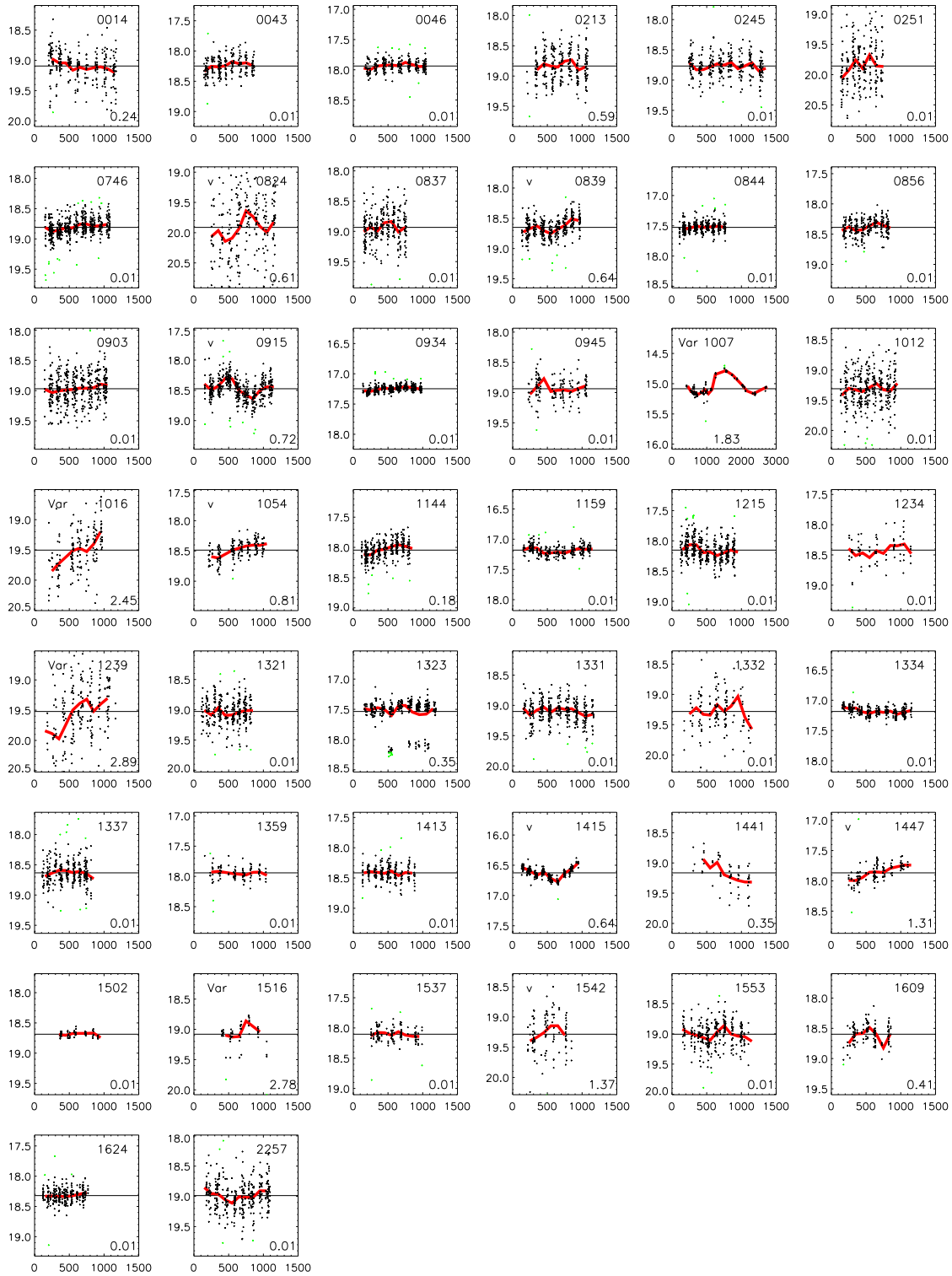


Figure 13. Optical continuum magnitude for BAL RLQs (labeled by truncated RA), plotted versus rest-frame timescale where the zero point is at MJD 53000. The red line is a running mean within rest-frame 200 d bins after outlier rejection (green points omitted, black points retained). A measure of variability is printed at lower right for each object; see §4.2 for details. Objects with mild and strong variability are labeled as v and Var, respectively.

with lines). For RLQs the longest separation measurement is plotted with larger symbol size, while for RQQs only the longest separation measurement is plotted for clarity. For both RLQs and RQQs the velocity width of the varying regions tends to be only a few thousand km s^{-1} , as previously found for RQQs by Gibson et al. (2008). These and the previous results are consistent with a simple scenario in which component segments within a given BAL have a uniform and independent probability to vary, as could arise from moving material at different radial velocities passing transversely through the line of sight.

It would also be of interest to compare and contrast variability within the Si IV absorption region to that discussed here for C IV BALs. Unfortunately, our sample is selected in z for C IV coverage and several of these BAL RLQs do not have Si IV coverage, which makes a robust statistical comparison difficult. In RQQs, Si IV absorption may be more variable than C IV (Capellupo et al. 2012; but see also G10) and segments at similar velocities may show coordinated variability (G10; Capellupo et al. 2012); a larger sample (restricted to higher redshifts) could test whether this also holds for RLQs.

4.2 Optical continuum variability

We next investigate continuum variability in BAL quasars. One motivation for considering optical continuum variability is that it could be indicative of direct incident flux altering the absorber ionization state (e.g., Trevese et al. 2013) or covering factor. However, such potential connections are better explored with EUV or X-ray observations (e.g., Gallagher et al. 2004; Saez et al. 2012; Hamann et al. 2013), which directly probe the high-energy radiation relevant to BAL shielding and driving. Of greater relevance, a mutual origin of BAL outflows and optical emission in the accretion disk might link continuum and absorption line variability; for example, a particularly inhomogeneous disk in some quasars (e.g., speculatively due to near-Eddington accretion) might facilitate the launching of absorbing clumps that are then observable as BALs.

Optical magnitudes at multiple epochs were obtained from the Catalina Sky Survey¹⁰ (Drake et al. 2009), Data Release 2. These unfiltered CCD measurements of the quasar optical continua are plotted for BAL RLQs in Figure 13 and for BAL RQQs in Appendix B. The magnitudes are screened for outliers using two passes of 3σ rejection, after which the median magnitude is taken as the baseline brightness (dashed line in each frame). Timescales are converted to rest-frame with MJD 53000 as the fixed zero point (for reference, the DR2 release date for SDSS is 53079). The plots show a running mean calculated within rest-frame timescale bins of 200 d for bins containing at least 4 valid measurements (plotted as a solid red line).

We quantify optical continuum variability using a structure function, following the general approach of Rengstorf et al. (2006; see also Vanden Berk et al. 2004; di Clemente et al. 1996). In addition to comparing optical continuum variability in BAL RLQs versus BAL RQQs, we wish to test

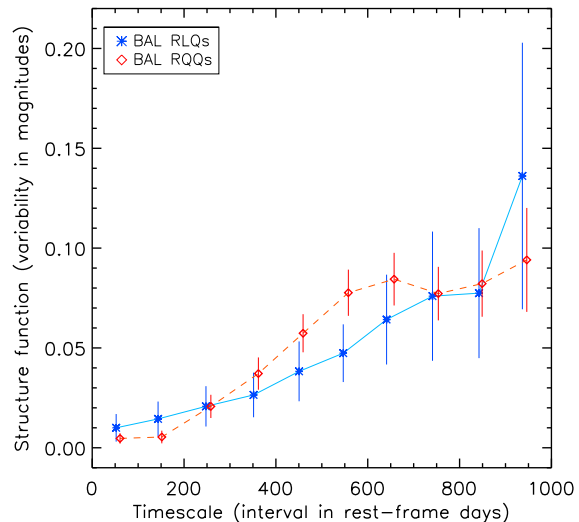


Figure 14. Optical continuum variability as a function of time lag for BAL RLQs (blue stars) and BAL RQQs (red diamonds). The structure function is calculated as detailed in §4.2. Both BAL RLQs and RQQs show greater variability on longer timescales, and tend toward similar variability for any given interval.

whether optical continuum variability is linked to BAL variability. Given the high-cadence but irregular monitoring of the Catalina Sky Survey and the desired application of a uniform procedure for assessing variability within each BAL quasar, we choose to bin the σ -clipped magnitudes within intervals of 20 rest-frame days (here we are only interested in variability on longer timescales) prior to calculating the structure function. Errors within each bin are estimated including both the provided measurement uncertainties and the empirical scatter and then additionally enhanced by 30%. This slight initial smoothing and conservative inflation of errors does not impact the relative ranking between individual objects or the BAL RLQs versus BAL RQQs comparison but may give somewhat lower absolute structure function values than other approaches. The structure function is then considered for time lags up to 1000 rest-frame days, binned by 100 days. For each individual quasar, the sum of these 10 measurements (or weighted for truncated coverage) is used to quantify optical continuum variability, and these values are listed in Figure 13 and Appendix B.

The structure functions for BAL RLQs and for BAL RQQs averaged across objects (rather than across raw magnitude measurements) are given in Figure 14. The previously known tendency for quasars to display greater variability on longer timescales (e.g., above references) is clearly also present for BAL quasars, both RLQs and RQQs. There does not appear to be a significant difference between BAL RLQs and BAL RQQs in optical continuum variability (see Figure 14; if anything, BAL RLQs may be less variable). The mean continuum variability for BAL RLQs (for consistency again filtering out objects with $\langle EW \rangle < 3.5 \text{ \AA}$) is 0.37 ± 0.11 , similar to the value of 0.47 ± 0.07 for BAL RQQs. From 41 BAL RLQs, 7 (3) or 17% (7%) show mild (strong) continuum variability; in comparison, from 85 BAL RQQs, 22 (7) or 26% (8%) show mild (strong) continuum variability.

¹⁰ <http://nessi.cacr.caltech.edu/DataRelease/>

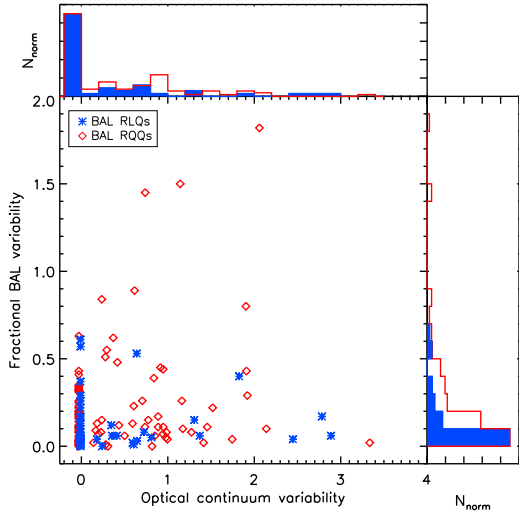


Figure 15. Optical continuum variability versus BAL variability for BAL RLQs (blue stars) and BAL RQQs (red diamonds). There is no apparent correlation. The one-dimensional variability distributions (shown as peak-normalized histograms) are similar, with BAL RLQs perhaps slightly less variable by both metrics.

We find no significant correlation between optical continuum and BAL variability (Table 6 and Figure 15).

Several previous studies have identified a tendency for RLQs to be more variable than are RQQs (e.g., Vanden Berk et al. 2004; Garcia et al. 1999; and references therein). We speculate that those samples include a substantial number of RLQs for which the inclination is close to the line of sight (including blazars) and that some of the variability in such RLQs may be jet-linked. The similarity between BAL RLQs and BAL RQQs might then support some geometric dependence to BAL outflows (i.e., our RLQs are not viewed down the jet). This is consistent with the intranight optical variability analysis of Joshi & Chand (2013), which found similar low variability in BAL RLQs and BAL RQQs. Regardless of the underlying physical explanation, the optical continuum results further support that variability in BAL RLQs is similar to (or modestly less than) that in BAL RQQs.

4.3 Influence of radio properties

The absolute change and absolute fractional change in equivalent width are plotted versus radio luminosity and radio loudness in Figure 16. No strong dependencies of BAL variability upon radio properties are apparent. The median and mean values of $|\Delta EW|$, or $|\Delta EW|/\langle EW \rangle$ are similar for RLQs split at either $\ell_r = 33$ or $R^* = 2$, and KS tests find no significant differences in their distributions (Table 5). This is confirmed by Kendall and Spearman correlation tests (Table 6), which show no significant correlation (probability < 0.5 in all cases) of $|\Delta EW|$ or $|\Delta EW|/\langle EW \rangle$ with either ℓ_r or R^* . At most there is a very slight tendency, not statistically significant, for increased $|\Delta EW|/\langle EW \rangle$ toward higher R^* values. However, this may be influenced by the relatively large (within our sample) $|\Delta EW|/\langle EW \rangle$ values of a few lobe-dominated quasars, for which the R^* values tend to

be high (Figure 16) and might indeed be somewhat overestimated due to inclusion of lobe emission or intrinsic reddening depressing the optical continuum. Groupings of RLQs divided by $\Delta\tau$ or $\langle EW \rangle$ also do not show any significant trends, with the exception of an apparent anti-correlation between $|\Delta EW|$ and R^* for RLQs with $\langle EW \rangle > 20 \text{ \AA}$ that may again be related to sample inhomogeneity (in this case, two varying RLQs that have large $\Delta\tau$ timescales).

It may be noted from Figure 16 that the lobe-dominated RLQs tend toward greater fractional variability than the core-dominated RLQs. Indeed, the mean $|\Delta EW|/\langle EW \rangle$ is 0.24 ± 0.07 (0.09 ± 0.02) for lobe-dominated (core-dominated) RLQs, and KS tests support marginal ($p = 0.04$) inconsistency. However, the small number of lobe-dominated BAL RLQs in our sample, as well as their generally greater $\Delta\tau$ and smaller $\langle EW \rangle$ values (median 1500 d versus 600 d and 11 \AA versus 20 \AA , respectively), indicates additional study is required to confirm these conclusions. Anecdotally, other cases of notable BAL variability in lobe-dominated RLQs are known; for example, Hall et al. (2011) report dramatic variability in the Mg II and Fe II absorption features in the lobe-dominated RLQ FBQS J1408+3054 (the redshift of $z = 0.848$ precludes optical coverage of the C IV region; this is a “FeLoBAL” object that shows absorption within lower ionization features, in this case including iron).

Studies of the radio spectral indices of non-BAL and BAL RLQs have found that BAL RLQs tend to have steeper values of α_r , suggestive of greater inclinations to the line of sight (DiPompeo et al. 2012; Bruni et al. 2012). This is consistent with a geometrical dependence to BAL structure, although it does appear that outflows can exist at equatorial-to-polar latitudes. Within our sample, there is no strong dependence between α_r and BAL variability in core-dominated BAL RLQs; lobe-dominated RLQs, with generally steep radio spectral indices, may tend toward somewhat greater absorption variability as discussed above.

4.4 Relevance to outflow models

In a disk-wind scenario, outflows launched from a rotating disk could maintain an approximately Keplerian transverse velocity while traveling radially, and consequent changes in the covering factor as clouds move across the (extended) source can provide an explanation for the observed minor shifts in depths at constant line-of-sight velocity that characterize BAL variability in RQQs (Gibson et al. 2008; G10; Capellupo et al. 2012). If lobe-dominated RLQs, known to be more inclined than core-dominated RLQs, indeed show enhanced BAL variability, then (particularly given the lack of correlation between variability and general radio properties) this requires some geometrical dependence of the BAL outflow structure. The very presence of BALs in flat-spectrum, core-dominated RLQs is likely incompatible with a strictly equatorial outflow¹¹, but simulations of line-driven disk winds indicate that material may be ejected at a range of angles relative to the accretion disk (e.g., Giustini & Proga 2012). For the BAL RLQs considered here, it appears

¹¹ Note, however, determination of BAL RLQs as possessing polar outflows based solely on radio variability and inferred brightness temperature may be problematic (Hall & Chajet 2011).

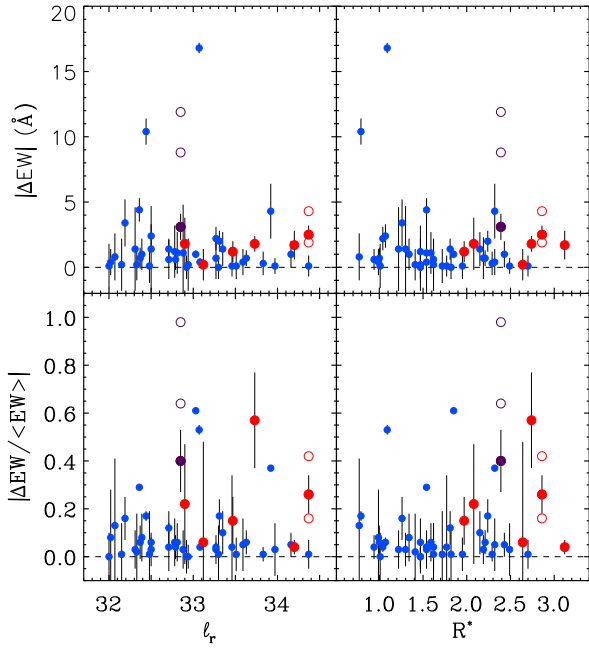


Figure 16. Absolute change in BAL equivalent width and absolute fractional change in BAL equivalent width versus radio luminosity (left) and radio loudness (right) for BAL RLQs. Core-dominated and lobe-dominated objects are plotted as smaller blue and larger red circles, respectively (with the lobe-dominated PG 1004+130 in purple; here and for SDSS J004323.43001552.4 shorter-separation measurements are shown as open circles). There are no obvious strong trends with ℓ_r or R^* . The lobe-dominated RLQs tend to display greater absolute and fractional variability than the core-dominated objects.

unnecessary to invoke an evolutionary phase, in which the quasar is nearly completely enshrouded, to explain the presence of BALs. Recall, however, that our sample is composed almost exclusively of HiBALs, and LoBALs may have distinct properties (§1; White et al. 2007).

The lack of any apparent correlation between BAL variability and (core plus lobe) radio loudness or luminosity would seem to suggest that the strength of the jet does not exercise a controlling influence upon the absorbing outflow. While the scarcity of BAL RLQs with both high values of R^* and large C IV absorption EW (Figure 1) could indicate a physical connection (see also Shankar et al. 2008 for modeling of the radio-loud and BAL fractions), it might alternatively be due simply to a low likelihood for any given object to possess, independently, extreme radio and BAL properties. If the jet and wind are not intimately connected in BAL RLQs, this provides an interesting contrast with the situation for X-ray binaries, for which it is found that the jet-aided development of a radiation-driven wind can remove sufficient material to starve a jet (e.g., Neilsen & Lee 2009), in a feedback cycle between the “low/hard” and “high/soft” states. The longer timescales (scaling with black hole mass) in quasars, perhaps in concert with a greater influence of the corona upon the accretion structure than operates in X-ray binaries, appear to permit dual-mode feedback with both the high-velocity, low-mass jets and the relatively lower-velocity, higher-mass winds (e.g., Proga et al. 2010) capable of signif-

icant energy injection into their surroundings. If indeed mechanical power is ejected primarily in the form of jets below $L_{\text{bol}} \sim 10^{-2} L_{\text{Edd}}$ and as winds at higher accretion luminosities (King et al. 2013), RLQs may sit near this boundary. RLQs also hosting BALs¹² might therefore be expected to be particularly efficient at quenching star-formation within their host galaxies.

5 SUMMARY

We have carried out a study of C IV BAL variability within a representative sample of 46 RLQs, using 78 pairs of spectra collected with rest-frame separations of 80–6000 d. Our primary results are the following:

1. Changes in BAL structure are generally either modest or statistically insignificant; the mean absolute fractional change $|\Delta EW|/\langle EW \rangle$ is 0.10 ± 0.02 , somewhat lower than the 0.17 ± 0.03 found in a matched sample of BAL RQQs. BAL variability in RLQs, where observed, typically consists of a slight change in the depth of a portion of the absorption trough, qualitatively similar to BAL RQQ variability (see §3.2, 4.1, Table 5, Appendix A).

2. BALs in RLQs vary more on longer timescales (as do BALs in RQQs). The absolute fractional change in equivalent width is correlated with $\Delta\tau$, and the mean $|\Delta EW|/\langle EW \rangle$ is 0.13 ± 0.03 (0.06 ± 0.02) for $\Delta\tau \geq 500$ d (< 500 d) (see §4.1, Table 5, Figure 10).

3. BALs of larger equivalent width tend to show greater absolute (but not fractional) changes in equivalent width, for both RLQs and RQQs, perhaps due to their coverage of more discrete velocity segments (see §4.1, Table 6, Figure 11).

4. BAL RLQs and BAL RQQs show similar optical continuum variability patterns (if anything, BAL RLQs are less variable) and both vary more on longer timescales, in common with non-BAL quasars (see §4.2, Figures 13–14, Appendix B).

5. Radio loudness and luminosity do not influence BAL variability. The mean $|\Delta EW|$ and $|\Delta EW|/\langle EW \rangle$ values for RLQs divided at $R^* = 2$ or $\ell_r = 33$ are similar, and neither measure of BAL variability is significantly correlated with either R^* or ℓ_r for these BAL RLQs (see §4.3, Table 6).

6. Lobe-dominated RLQs apparently show greater fractional BAL variability than do core-dominated RLQs: the mean $|\Delta EW|/\langle EW \rangle$ is 0.24 ± 0.07 (0.09 ± 0.02) for lobe-dominated (core-dominated) RLQs. However, the small number of lobe-dominated BAL RLQs in our sample, as well as their generally greater $\Delta\tau$ and smaller $\langle EW \rangle$ values here, indicates additional study is warranted to confirm these conclusions (see §4.3, Figure 16).

In summary, BAL variability in RLQs appears to occur in a similar manner as in RQQs (consistent with a common physical mechanism, such as a disk wind), but at perhaps weaker amplitude or with lesser frequency. The lack of dependence upon radio properties suggests that the jet in RLQs does not strongly influence the absorber, while the potential greater variability in lobe-dominated objects supports some geometrical dependence to the outflow structure.

¹² If BALs in RLQs are only detectable along a particular line of sight, the intrinsic fraction of RLQs hosting BALs could be much larger than observed.

6 ACKNOWLEDGMENTS

We thank Mike Eracleous, Karen Lewis, and Paola Rodríguez Hidalgo for helpful conversations and suggestions, Mike Brotherton for providing a spectrum for J1016, and Paul Martini for assistance with OSMOS. We thank the anonymous referee for a thoughtful and constructive report that improved this paper. This work was partially conducted by CAW through the Research Experiences for Undergraduates program at the College of Wooster. WNB acknowledges NSF grant AST 1108604 and NASA ADP grant NNX10AC99G.

This project made use of the NRAO VLA Archive Survey, (c) AUI/NRAO. The NVAS can currently be browsed through <http://www.aoc.nrao.edu/~vlbacald/>.

This research has made use of the NASA/IPAC Extragalactic Database (NED) which is operated by the Jet Propulsion Laboratory, California Institute of Technology, under contract with the National Aeronautics and Space Administration.

The CSS survey is funded by the National Aeronautics and Space Administration under Grant No. NNG05GF22G issued through the Science Mission Directorate Near-Earth Objects Observations Program. The CRTS survey is supported by the U.S. National Science Foundation under grants AST-0909182.

Funding for the SDSS and SDSS-II has been provided by the Alfred P. Sloan Foundation, the Participating Institutions, the National Science Foundation, the U.S. Department of Energy, the National Aeronautics and Space Administration, the Japanese Monbukagakusho, the Max Planck Society, and the Higher Education Funding Council for England. The SDSS Web Site is <http://www.sdss.org/>.

The Hobby-Eberly Telescope (HET) is a joint project of the University of Texas at Austin, the Pennsylvania State University, Stanford University, Ludwig-Maximilians-Universität München, and Georg-August-Universität Göttingen. The HET is named in honor of its principal benefactors, William P. Hobby and Robert E. Eberly. The Marcario Low-Resolution Spectrograph is named for Mike Marcario of High Lonesome Optics, who fabricated several optics for the instrument but died before its completion; it is a joint project of the Hobby-Eberly Telescope partnership and the Instituto de Astronomía de la Universidad Nacional Autónoma de México.

REFERENCES

Arav, N., & Begelman, M. C. 1994, *ApJ*, 434, 479
 Arav, N., Borguet, B., Chamberlain, C., Edmonds, D., & Danforth, C. 2013, [arXiv:1305.2181](https://arxiv.org/abs/1305.2181)
 Barlow, T. A. 1993, Ph.D. Thesis
 Becker, R. H., White, R. L., & Helfand, D. J. 1995, *ApJ*, 450, 559
 Becker, R. H., Gregg, M. D., Hook, I. M., McMahon, R. G., White, R. L., & Helfand, D. J. 1997, *ApJL*, 479, L93
 Becker, R. H., White, R. L., Gregg, M. D., Brotherton, M. S., Laurent-Muehleisen, S. A., & Arav, N. 2000, *ApJ*, 538, 72
 Becker, R. H., et al. 2001, *ApJS*, 135, 227
 Benn, C. R., Carballo, R., Holt, J., Vigotti, M., González-Serrano, J. I., Mack, K.-H., & Perley, R. A. 2005, *MNRAS*, 360, 1455
 Brandt, W. N., Laor, A., & Wills, B. J. 2000, *ApJ*, 528, 637
 Brotherton, M. S., van Breugel, W., Smith, R. J., Boyle, B. J.,

Shanks, T., Croom, S. M., Miller, L., & Becker, R. H. 1998, *ApJL*, 505, L7
 Brotherton, M. S., De Breuck, C., & Schaefer, J. J. 2006, *MNRAS*, 372, L58
 Brotherton, M. S., De Breuck, C., & Schaefer, J. J. 2011, *MNRAS*, L223
 Bruni, G., Mack, K.-H., Salerno, E., et al. 2012, *A&A*, 542, A13
 Bruni, G., Dallacasa, D., Mack, K.-H., et al. 2013, *A&A*, 554, A94
 Capellupo, D. M., Hamann, F., Shields, J. C., Rodríguez Hidalgo, P., & Barlow, T. A. 2011, *MNRAS*, 131
 Capellupo, D. M., Hamann, F., Shields, J. C., Rodríguez Hidalgo, P., & Barlow, T. A. 2012, *MNRAS*, 422, 3249
 Capellupo, D. M., Hamann, F., Shields, J. C., Halpern, J. P., & Barlow, T. A. 2013, *MNRAS*, 429, 1872
 Chartas, G., Eracleous, M., Agol, E., & Gallagher, S. C. 2004, *ApJ*, 606, 78
 de Vries, W. H., Becker, R. H., & White, R. L. 2006, *AJ*, 131, 666
 di Clemente, A., Giallongo, E., Natali, G., Trevese, D., & Vagnetti, F. 1996, *ApJ*, 463, 466
 DiPompeo, M. A., Brotherton, M. S., & De Breuck, C. 2011, *ApJS*, 193, 9
 DiPompeo, M. A., Brotherton, M. S., & De Breuck, C. 2012, *ApJ*, 752, 6
 DiPompeo, M. A., Runnoe, J. C., Brotherton, M. S., & Myers, A. D. 2013, *ApJ*, 762, 111
 Drake, A. J., Djorgovski, S. G., Mahabal, A., et al. 2009, *ApJ*, 696, 870
 Filiz Ak, N., Brandt, W. N., Hall, P. B., et al. 2012, *ApJ*, 757, 114
 Filiz Ak, N., Brandt, W. N., Hall, P. B., et al. 2013, *ApJ*, 777, 168
 Gallagher, S. C., Brandt, W. N., Wills, B. J., et al. 2004, *ApJ*, 603, 425
 Gallagher, S. C., Brandt, W. N., Chartas, G., Priddey, R., Garmire, G. P., & Sambruna, R. M. 2006, *ApJ*, 644, 709
 Gallagher, S. C., Hines, D. C., Blaylock, M., Priddey, R. S., Brandt, W. N., & Egami, E. E. 2007, *ApJ*, 665, 157
 Ganguly, R., Brotherton, M. S., Cales, S., et al. 2007, *ApJ*, 665, 990
 Garcia, A., Sodr e, L., Jablonski, F. J., & Terlevich, R. J. 1999, *MNRAS*, 309, 803
 Gibson, R. R., Brandt, W. N., Schneider, D. P., & Gallagher, S. C. 2008, *ApJ*, 675, 985
 Gibson, R. R., Brandt, W. N., Gallagher, S. C., & Schneider, D. P. 2009a, *ApJ*, 696, 924
 Gibson, R. R., et al. 2009b, *ApJ*, 692, 758 (G09)
 Gibson, R. R., Brandt, W. N., Gallagher, S. C., Hewett, P. C., & Schneider, D. P. 2010, *ApJ*, 713, 220
 Giustini, M., & Proga, D. 2012, *ApJ*, 758, 70
 Glikman, E., Urrutia, T., Lacy, M., et al. 2012, *ApJ*, 757, 51
 Gopal-Krishna, & Wiita, P. J. 2000, *A&A*, 363, 507
 Gregg, M. D., Becker, R. H., Brotherton, M. S., Laurent-Muehleisen, S. A., Lacy, M., & White, R. L. 2000, *ApJ*, 544, 142
 Gregg, M. D., Becker, R. H., & de Vries, W. 2006, *ApJ*, 641, 210
 Hall, P. B., Sadavoy, S. I., Hutsemekers, D., Everett, J. E., & Rafiee, A. 2007, *ApJ*, 665, 174
 Hall, P. B., Anosov, K., White, R. L., Brandt, W. N., Gregg, M. D., Gibson, R. R., Becker, R. H., & Schneider, D. P. 2011, *MNRAS*, 411, 2653
 Hall, P. B., & Chajet, L. S. 2011, [arXiv:1105.1689](https://arxiv.org/abs/1105.1689)
 Hall, P. B., Brandt, W. N., Petitjean, P., et al. 2013, *MNRAS*, 434, 222
 Hamann, F., Chartas, G., McGraw, S., et al. 2013, *MNRAS*, 435, 133
 Hazard, C., Morton, D. C., Terlevich, R., & McMahon, R. 1984, *ApJ*, 282, 33
 Hewett, P. C., & Foltz, C. B. 2003, *AJ*, 125, 1784

- Hewett, P. C., & Wild, V. 2010, *MNRAS*, 405, 2302
- Hill, G. J., Nicklas, H. E., MacQueen, P. J., Tejada, C., Cobos Duenas, F. J., & Mitsch, W. 1998, *Proc. SPIE*, 3355, 375
- Joshi, R., & Chand, H. 2013, *MNRAS*, 429, 1717
- Kimball, A. E., Ivezić, Ž., Wiita, P. J., & Schneider, D. P. 2011, *AJ*, 141, 182
- King, A. L., Miller, J. M., Raymond, J., et al. 2013, *ApJ*, 762, 103
- Laor, A., & Brandt, W. N. 2002, *ApJ*, 569, 641
- Liu, Y., Jiang, D. R., Wang, T. G., & Xie, F. G. 2008, *MNRAS*, 391, 246
- Lundgren, B. F., Wilhite, B. C., Brunner, R. J., Hall, P. B., Schneider, D. P., York, D. G., Vanden Berk, D. E., & Brinkmann, J. 2007, *ApJ*, 656, 73
- Luo, B., Brandt, W. N., Alexander, D. M., et al. 2013, *arXiv:1306.3500*
- Menou, K., et al. 2001, *ApJ*, 561, 645
- Misawa, T., Eracleous, M., Charlton, J. C., & Tajitsu, A. 2005, *ApJ*, 629, 115
- Miller, B. P., Brandt, W. N., Gallagher, S. C., et al. 2006, *ApJ*, 652, 163
- Miller, B. P., Brandt, W. N., Gibson, R. R., Garmire, G. P., & Shemmer, O. 2009, *ApJ*, 702, 911
- Miller, B. P., Welling, C. A., Brandt, W. N., & Gibson, R. R. 2012, *AGN Winds in Charleston*, 460, 118
- Montenegro-Montes, F. M., Mack, K. -, Benn, C. R., Carballo, R., Dallacasa, D., González-Serrano, J. I., Holt, J., & Jiménez-Luján, F. 2009, *arXiv:0903.5119*
- Murray, N., Chiang, J., Grossman, S. A., & Voit, G. M. 1995, *ApJ*, 451, 498
- Narayanan, D., Hamann, F., Barlow, T., Burbidge, E. M., Cohen, R. D., Junkkarinen, V., & Lyons, R. 2004, *ApJ*, 601, 715
- Neilsen, J., & Lee, J. C. 2009, *Nature*, 458, 481
- Netzer, H., Chelouche, D., George, I. M., et al. 2002, *ApJ*, 571, 256
- Ogle, P. M., Cohen, M. H., Miller, J. S., Tran, H. D., Goodrich, R. W., & Martel, A. R. 1999, *ApJS*, 125, 1
- Proga, D., Stone, J. M., & Kallman, T. R. 2000, *ApJ*, 543, 686
- Proga, D., Kurosawa, R., & Nagamine, K. 2010, *IAU Symposium*, 267, 354
- Proga, D., Rodríguez-Hidalgo, P., & Hamann, F. 2012, *AGN Winds in Charleston*, 460, 171
- Ramsey, L. W., et al. 1998, *Proc. SPIE*, 3352, 34
- Rengstorf, A. W., Brunner, R. J., & Wilhite, B. C. 2006, *AJ*, 131, 1923
- Richards, G. T., Kruczek, N. E., Gallagher, S. C., et al. 2011, *AJ*, 141, 167
- Risaliti, G., Elvis, M., & Nicastro, F. 2002, *ApJ*, 571, 234
- Rodríguez Hidalgo, P., Hamann, F., Eracleous, M., et al. 2012, *arXiv:1203.3830*
- Rodríguez Hidalgo, P., Eracleous, M., Charlton, J., et al. 2013, *ApJ*, 775, 14
- Saez, C., Brandt, W. N., Gallagher, S. C., Bauer, F. E., & Garmire, G. P. 2012, *ApJ*, 759, 42
- Schneider, D. P., et al. 2005, *AJ*, 130, 367
- Schneider, D. P., et al. 2007, *AJ*, 134, 102
- Schneider, D. P., et al. 2010, *AJ*, 139, 2360
- Shankar, F., Dai, X., & Sivakoff, G. R. 2008, *ApJ*, 687, 859
- Sim, S. A., Proga, D., Kurosawa, R., et al. 2012, *MNRAS*, 426, 2859
- Stawarz, L., Ostorero, L., Begelman, M. C., Moderski, R., Kataoka, J., & Wagner, S. 2008, *ApJ*, 680, 911
- Stocke, J. T., Morris, S. L., Weymann, R. J., & Foltz, C. B. 1992, *ApJ*, 396, 487
- Trevese, D., Saturni, F. G., Vagnetti, F., et al. 2013, *A&A*, 557, A91
- Trump, J. R., et al. 2006, *ApJS*, 165, 1
- Urrutia, T., Lacy, M., & Becker, R. H. 2008, *ApJ*, 674, 80
- Urrutia, T., Becker, R. H., White, R. L., Glikman, E., Lacy, M., Hodge, J., & Gregg, M. D. 2009, *ApJ*, 698, 1095
- Vanden Berk, D. E., et al. 2001, *AJ*, 122, 549
- Vanden Berk, D. E., Wilhite, B. C., Kron, R. G., et al. 2004, *ApJ*, 601, 692
- Venturini, S., & Solomon, P. M. 2003, *ApJ*, 590, 740
- Weymann, R. J., Carswell, R. F., & Smith, M. G. 1981, *ARAA*, 19, 41
- Weymann, R. J., Morris, S. L., Foltz, C. B., & Hewett, P. C. 1991, *ApJ*, 373, 23
- White, R. L., Becker, R. H., Gregg, M. D., et al. 2000, *ApJS*, 126, 133
- White, R. L., Helfand, D. J., Becker, R. H., Glikman, E., & de Vries, W. 2007, *ApJ*, 654, 99
- Willott, C. J., Rawlings, S., & Grimes, J. A. 2003, *ApJ*, 598, 909
- Wills, B. J., & Brotherton, M. S. 1995, *ApJL*, 448, L81
- Wills, B. J., Brandt, W. N., & Laor, A. 1999, *ApJL*, 520, L91
- Wu, J., Brandt, W. N., Comins, M. L., et al. 2010, *ApJ*, 724, 762
- York, D. G., et al. 2000, *AJ*, 120, 1579
- Young, S., Axon, D. J., Robinson, A., Hough, J. H., & Smith, J. E. 2007, *Nature*, 450, 74
- Yuan, M. J., & Wills, B. J. 2003, *ApJL*, 593, L11
- Zhang, S., Wang, T.-G., Wang, H., et al. 2010, *ApJ*, 714, 367
- Zhou, H., Wang, T., Wang, H., et al. 2006, *ApJ*, 639, 716

Table 1. BAL RLQs: radio and optical properties and longest-separation summed BAL measurements

Name (SDSS J2000)	z	m_i	M_i	ℓ_{UV}^a	ℓ_r	R^*	$\Delta(g-i)^b$	$\Delta\tau^c$	$\langle EW \rangle^d$	ΔEW^e	$\frac{ \Delta EW }{\langle EW \rangle} f$	Notes ^g
001438.28–010750.1	1.806	18.36	–26.77	30.99	32.00	1.01	0.59	258	16.2	–0.1±1.7	0.00	
004323.43–001552.4	2.798	18.15	–27.96	31.51	34.37	2.86	0.38	675	9.4	–2.5±0.7	0.26	LD
004613.54+010425.7	2.152	17.77	–27.76	31.43	32.50	1.07	0.31	1881	39.5	–2.4±0.9	0.06	
021333.34+003030.8	2.053	18.90	–26.52	30.92	32.33	1.41	0.80	854	7.6	–0.2±1.2	0.02	
024534.07+010813.7	1.536	18.37	–26.38	30.76	32.48	1.72	0.67	436	7.5	+0.1±1.3	0.01	
025105.14–001732.1	3.456	19.53	–27.05	31.30	32.07	0.77	0.66	69	6.4	+0.8±1.8	0.13	
074610.50+230710.7	2.093	18.27	–27.20	31.20	33.35	2.15	1.06	624	14.5	+1.4±1.3	0.10	FS
082450.19+440212.8	1.866	19.59	–25.61	30.53	32.15	1.62	0.25	87	15.0	+0.2±2.0	0.01	
083749.59+364145.5	3.416	18.54	–28.02	31.54	33.83	2.29	0.61	496	33.2	–0.3±0.9	0.01	
083925.61+045420.2	2.447	18.30	–27.52	31.34	32.88	1.54	1.80	17	44.8	–1.1±3.7	0.03	Lo
084401.95+050357.9	3.346	17.01	–29.50	32.23	33.27	1.04	1.10	420	57.1	+2.2±0.9	0.04	
085641.56+424253.9	3.062	18.42	–27.90	31.42	33.63	2.21	0.07	546	11.2	–0.7±0.6	0.06	FS
090306.67+272532.9	2.233	18.86	–26.75	31.05	32.39	1.34	0.45	319	11.7	+1.0±1.2	0.08	
091512.53+305014.9	1.983	18.54	–26.80	31.03	32.02	0.99	0.35	130	4.8	–0.4±1.0	0.08	
093403.96+315331.3	2.422	17.07	–28.73	31.85	32.79	0.94	0.80	300	17.2	+0.6±0.8	0.04	
094513.89+505521.8	2.137	18.59	–26.93	31.09	32.31	1.22	0.97	672	42.8	–1.4±3.2	0.03	Lo
100726.10+124856.2	0.241	15.17	–25.12	30.46	32.85	2.39	–0.51	6163	7.8	–3.1±1.0	0.40	LD
101219.48+350333.8	2.628	19.02	–26.96	31.20	32.50	1.30	0.74	114	50.1	–1.4±3.3	0.03	
101614.26+520915.7	2.460	19.23	–26.62	31.08	34.20	3.12	1.39	1198	41.1	–1.7±1.1	0.04	LD
105416.51+512326.0	2.340	18.47	–27.25	31.27	33.59	2.32	0.35	549	9.1	+0.4±1.0	0.05	FS
114436.65+095904.9	3.150	18.07	–28.31	31.69	33.46	1.77	0.21	419	2.5	–0.1±0.8	0.04	
115944.82+011206.9	2.002	16.98	–28.39	31.67	34.37	2.70	0.40	952	12.7	+0.1±0.8	0.01	J, MB?
121539.66+090607.4	2.723	18.09	–27.97	31.60	33.92	2.32	0.18	1571	11.6	–4.3±2.1	0.37	
123411.74+615832.5	1.949	18.37	–26.93	31.08	33.27	2.19	0.46	745	28.6	–0.7±1.6	0.03	
123954.15+373954.5	1.841	19.70	–25.47	30.48	33.12	2.64	0.41	770	2.8	+0.2±1.2	0.06	LD, Lo
132139.86–004151.9	3.074	18.66	–27.66	31.47	32.94	1.47	1.46	77	39.9	–0.2±2.0	0.00	Lo
132304.58–003856.5	1.827	17.81	–27.34	31.22	32.81	1.59	0.53	113	19.3	–1.1±1.6	0.06	
133150.51+004518.8	1.885	18.89	–26.33	30.82	32.36	1.54	0.15	101	15.4	+4.4±0.9	0.29	
133259.16+490946.9	1.995	19.08	–26.27	30.82	32.90	2.08	1.15	503	8.0	+1.8±2.0	0.22	LD
133428.06–012349.0	1.876	16.80	–28.41	31.65	32.44	0.79	1.02	2027	60.3	–10.4±1.0	0.17	Lo
133701.39–024630.2	3.063	18.41	–27.91	31.48	33.97	2.49	0.18	512	5.1	–0.1±0.6	0.03	FS
135910.45+563617.3	2.248	17.76	–27.87	31.49	33.30	1.82	0.58	933	7.6	+0.0±0.9	0.01	
141151.97+550948.7	1.889	18.47	–26.76	30.99	33.73	2.74	0.18	929	3.1	–1.8±0.6	0.57	LD
141334.38+421201.7	2.818	18.23	–27.91	31.56	33.51	1.95	0.53	465	14.5	+0.1±1.0	0.01	J, FS
141546.24+112943.4	2.560	16.91	–29.02	31.98	33.07	1.09	0.29	1954	31.9	–16.8±0.4	0.53	Lo
144136.54+632519.4	1.779	18.55	–26.54	30.90	32.71	1.81	0.10	792	11.7	–1.4±0.8	0.12	
144707.40+520340.1	2.065	17.47	–27.96	31.50	33.47	1.97	0.44	486	7.6	+1.2±0.8	0.15	LD
150206.66–003606.9	2.200	18.47	–27.11	31.18	33.03	1.85	0.15	118	1.7	+1.0±0.3	0.61	
151630.30–005625.5	1.921	18.31	–26.96	31.08	33.31	2.24	0.39	1131	11.7	–2.0±0.8	0.17	
153703.95+533220.0	2.406	17.90	–27.88	31.54	33.08	1.54	0.20	20	10.3	+0.4±0.3	0.04	
154241.14+532204.3	2.983	19.11	–27.15	31.31	32.78	1.47	1.08	17	20.3	–1.2±2.0	0.06	
155355.38+324513.3	2.065	18.90	–26.54	30.93	32.19	1.26	0.44	473	21.0	–3.4±1.8	0.16	
160943.33+522550.9	2.723	18.59	–27.47	31.37	32.37	1.00	0.38	588	12.1	+0.7±0.8	0.06	
162453.47+375806.6	3.380	18.17	–28.37	31.73	34.16	2.43	0.22	396	20.6	–1.0±1.0	0.05	J, MB
225706.17–002532.8	1.985	18.40	–26.95	31.09	32.71	1.62	1.11	1318	14.3	–0.6±1.5	0.04	
235702.54–004824.0	3.013	18.68	–27.61	31.45	32.92	1.47	0.42	103	12.8	–0.0±0.9	0.00	

^a Monochromatic optical/UV or radio luminosities are given at rest-frame 2500 Å or 5 GHz, respectively, in units of $\text{erg s}^{-1} \text{Hz}^{-1}$, expressed as a logarithm. The radio loudness is calculated as $R^* = \ell_r - \ell_{\text{UV}}$.

^b The relative color $\Delta(g-i)$ is calculated as $g-i$ less the median value for quasars near that redshift. Redder objects have $\Delta(g-i) > 0$.

^c Rest-frame time between BAL measurements, in days.

^d Average equivalent width, in Å.

^e Change in equivalent width, in Å.

^f Absolute fractional change in equivalent width

^g Lo: known LoBAL; MB: mini-BAL present; LD: lobe-dominated; J: small-scale milliarcsecond jet; FS: flat radio spectrum

Table 2. Measurements of RLQ C IV absorption troughs

Object ^a	$\lambda_1 - \lambda_2$ ^b	MJD	EW (Å)	Obs ^c	Object	$\lambda_1 - \lambda_2$	MJD	EW (Å)	Obs		
0014	1525–1548	51795	16.29±1.18	S	1012	1440–1545	53357	50.76±2.98	S		
		52518	16.21±1.18	S			53771	49.35±1.36	S		
0043	1444–1499	51794	10.61±0.61	S	1016	1509–1554	51546	28.69±0.54	K		
		52199	12.46±0.58	S			55684	29.35±0.71	H		
		54356	8.13±0.36	H			1460–1503	51546	13.32±0.24	K	
0046	1449–1493	51794	24.22±0.54	S	1054	1521–1543	55684	10.93±0.55	H		
		52199	22.69±0.45	S			52669	8.93±0.79	S		
		55776	22.29±0.32	H			54504	9.35±0.65	H		
	1524–1542	51794	15.54±0.80	S			1144	1473–1486	52734	2.60±0.51	S
		52199	15.26±0.75	S					54472	2.49±0.58	H
0213	1535–1547	55776	15.29±0.65	H	1159	1533–1549	51663	12.62±0.58	S		
		51816	7.72±0.99	S			51930	12.57±0.58	S		
		54413	7.55±0.68	H			54509	12.72±0.49	H		
0245	1536–1547	51871	7.40±0.91	S	1234	1463–1505	52373	28.98±1.30	S		
		52177	7.92±1.10	S			54552	28.61±0.72	H		
		52973	7.51±0.99	S			54579	28.24±0.96	H		
0251	1522–1534	51871	6.00±1.24	S	1321	1488–1549	51665	40.03±1.48	S		
		52177	6.82±1.30	S			51984	39.87±1.34	S		
		52577	5.65±0.72	S			1323	1495–1511	51665	8.76±0.78	S
0746	1525–1537	54452	6.54±0.50	H	1332	1511–1530	51984	8.39±0.58	S		
		54507	6.63±0.66	S			1518–1535	51665	11.08±0.93	S	
		52577	8.14±0.65	S			51984	10.35±0.85	S		
	1539–1549	54452	8.48±0.66	H			52762	7.12±1.90	S		
		54507	8.54±0.65	S			54270	8.92±0.65	H		
0824	1518–1539	51959	14.89±1.49	S	1337	1528–1539	52427	5.13±0.42	S		
		52207	15.07±1.35	S			54504	5.00±0.36	H		
		52320	33.38±0.71	S			1359	1533–1549	52669	7.57±0.73	S
0837	1502–1543	54413	32.91±0.83	H	1411	1534–1544	55700	7.62±0.55	H		
		54452	33.57±0.69	H			53088	3.96±0.55	S		
		54504	33.10±0.49	H			55775	2.20±0.24	H		
0839	1417–1461	52650	21.20±1.50	S	1413	1529–1549	52823	14.45±0.84	S		
		52708	21.05±2.39	S			54594	14.54±0.58	H		
		52650	7.44±0.83	S			1415	1476–1535	53848	34.65±0.68	S
0839	1531–1554	52708	7.29±1.15	S	1441	1526–1542	54567	26.73±0.70	M		
		52650	16.75±1.06	S			55688	30.61±0.47	H		
		52708	15.91±1.56	S			52339	12.40±0.67	S		
0844	1412–1529	52650	56.04±0.65	S	1447	1447–1487	54533	10.95±0.50	S		
		54478	58.20±0.60	H			52786	7.00±0.58	S		
		52294	11.61±0.48	S			54271	8.17±0.51	H		
0856	1508–1527	54414	10.86±0.43	H	1516	1532–1552	52404	12.69±0.64	S		
		54520	10.88±0.38	H			55707	10.73±0.51	H		
		53387	11.23±0.96	S			1542	1525–1554	52374	20.85±1.49	S
0903	1491–1515	54416	12.21±0.71	H	1553	1476–1527	52442	19.66±1.40	S		
		53379	5.01±0.75	S			52825	22.67±1.56	S		
		53768	4.64±0.62	S			53227	19.42±1.26	S		
0934	1482–1499	53386	6.73±0.38	S	1609	1531–1547	54270	19.25±0.86	H		
		54414	6.92±0.29	H			52051	11.76±0.65	S		
		53386	10.15±0.48	S			54233	12.48±0.50	H		
0945	1405–1500	54414	10.60±0.48	H	1624	1403–1446	52767	15.32±0.55	S		
		52409	43.47±1.95	S			54270	14.20±0.42	H		
		54496	40.18±2.24	H			54504	14.25±0.49	H		
		54522	42.07±2.58	H			1528–1543	52767	5.82±0.47	S	
1007	1491–1532	45083	5.66±0.65	I	2257	1537–1554	54270	5.17±0.38	H		
		46442	14.04±0.82	I			54504	5.85±0.40	H		
		52729	3.66±0.36	T			51792	14.63±1.21	S		
		1537–1552	45083	3.67±0.52			I	52178	14.19±1.18	S	
			46442	4.09±0.46			I	55740	14.01±0.80	H	
2357	1525–1541	52729	2.54±0.31	T	2357	1525–1541	51791	12.82±0.58	S		
							52203	12.77±0.70	S		

^a Truncated, see Table 1 for full name.

^b Wavelength boundaries (in Å) of BAL; see §3.2 for details.

^c Observations from S: Sloan Digital Sky Survey; H: Hobby Eberly Telescope; I: International Ultraviolet Explorer; T: Hubble Space Telescope; M: MDM Observatory

Table 3. Variability of RLQ C IV absorption troughs

Name ^a	$\lambda_1 - \lambda_2$ (Å)	$\Delta\tau$ (d)	$\langle EW \rangle$ (Å)	ΔEW (Å)	$\frac{ \Delta EW }{\langle EW \rangle}$	Name	$\lambda_1 - \lambda_2$ (Å)	$\Delta\tau$ (d)	$\langle EW \rangle$ (Å)	ΔEW (Å)	$\frac{ \Delta EW }{\langle EW \rangle}$
0014	1525–1548	258	16.2	-0.1±1.7	0.00±0.10	1007	1537–1552	6163	3.1	-1.1±0.6	0.36±0.20
0043	1444–1499	675	9.4	-2.5±0.7	0.26±0.08			1095	3.9	+0.4±0.7	0.11±0.18
		107	11.5	+1.9±0.8	0.16±0.07			5068	3.3	-1.6±0.6	0.47±0.17
		568	10.3	-4.3±0.7	0.42±0.07	1012	1440–1545	114	50.1	-1.4±3.3	0.03±0.07
0046	1449–1493	1264	23.3	-1.9±0.6	0.08±0.03	1016	1509–1554	1198	29.0	+0.7±0.9	0.02±0.03
		129	23.5	-1.5±0.7	0.07±0.03		1460–1503	1198	12.1	-2.4±0.6	0.20±0.05
		1136	22.5	-0.4±0.6	0.02±0.02	1054	1521–1543	549	9.1	+0.4±1.0	0.05±0.11
	1524–1542	1264	15.4	-0.2±1.0	0.02±0.07	1144	1473–1486	419	2.5	-0.1±0.8	0.04±0.30
		129	15.4	-0.3±1.1	0.02±0.07	1159	1533–1549	952	12.7	+0.1±0.8	0.01±0.06
		1136	15.3	+0.0±1.0	0.00±0.06			89	12.6	-0.1±0.8	0.00±0.07
0213	1535–1547	854	7.6	-0.2±1.2	0.02±0.16			862	12.6	+0.2±0.8	0.01±0.06
0245	1536–1547	436	7.5	+0.1±1.3	0.01±0.18	1234	1463–1505	745	28.6	-0.7±1.6	0.03±0.06
		121	7.7	+0.5±1.4	0.07±0.19			736	28.8	-0.4±1.5	0.01±0.05
		315	7.7	-0.4±1.5	0.05±0.19			9	28.4	-0.4±1.2	0.01±0.04
0251	1522–1534	69	6.4	+0.8±1.8	0.13±0.28	1321	1488–1549	77	39.9	-0.2±2.0	0.00±0.05
0746	1525–1537	624	6.1	+1.0±1.0	0.16±0.16	1323	1495–1511	113	8.6	-0.4±1.0	0.04±0.11
		606	6.1	+0.9±0.9	0.15±0.14		1518–1535	113	10.7	-0.7±1.3	0.07±0.12
		18	6.6	+0.1±0.8	0.01±0.13	1332	1511–1530	503	8.0	+1.8±2.0	0.22±0.25
	1539–1549	624	8.3	+0.4±0.9	0.05±0.11	1337	1528–1539	512	5.1	-0.1±0.6	0.03±0.11
		606	8.3	+0.3±0.9	0.04±0.11	1359	1533–1549	933	7.6	+0.0±0.9	0.01±0.12
		18	8.5	+0.1±0.9	0.01±0.11	1411	1534–1544	929	3.1	-1.8±0.6	0.57±0.20
0824	1518–1539	87	15.0	+0.2±2.0	0.01±0.13	1413	1529–1549	465	14.5	+0.1±1.0	0.01±0.07
0837	1502–1543	496	33.2	-0.3±0.9	0.01±0.03	1415	1476–1535	518	32.6	-4.0±0.8	0.12±0.03
		21	33.0	+0.2±1.0	0.01±0.03			202	30.7	-7.9±1.0	0.26±0.03
		12	33.3	-0.5±0.8	0.01±0.03			316	28.7	+3.9±0.8	0.14±0.03
0839	1417–1461	17	21.1	-0.2±2.8	0.01±0.13	1441	1526–1542	792	11.7	-1.4±0.8	0.12±0.07
	1497–1509	17	7.4	-0.2±1.4	0.02±0.19	1447	1447–1487	486	7.6	+1.2±0.8	0.15±0.10
	1531–1554	17	16.3	-0.8±1.9	0.05±0.12	1516	1532–1552	1131	11.7	-2.0±0.8	0.17±0.07
0844	1412–1529	420	57.1	+2.2±0.9	0.04±0.02	1542	1525–1554	17	20.3	-1.2±2.0	0.06±0.10
0856	1508–1527	546	11.2	-0.7±0.6	0.06±0.05	1553	1476–1527	473	21.0	-3.4±1.8	0.16±0.09
		520	11.2	-0.8±0.6	0.07±0.06			132	21.0	-3.2±2.0	0.15±0.10
		26	10.9	+0.0±0.6	0.00±0.05			341	19.3	-0.2±1.5	0.01±0.08
0903	1491–1515	319	11.7	+1.0±1.2	0.08±0.10	1609	1531–1547	588	12.1	+0.7±0.8	0.06±0.07
0915	1535–1551	130	4.8	-0.4±1.0	0.08±0.20	1624	1403–1446	396	14.8	-1.1±0.7	0.07±0.05
0934	1482–1499	300	6.8	+0.2±0.5	0.03±0.07			343	14.8	-1.1±0.7	0.08±0.05
	1406–1440	300	10.4	+0.5±0.7	0.04±0.07			53	14.2	+0.1±0.6	0.00±0.05
0945	1405–1500	672	42.8	-1.4±3.2	0.03±0.08		1528–1543	396	5.8	+0.0±0.6	0.01±0.11
		664	41.8	-3.3±3.0	0.08±0.07			343	5.5	-0.7±0.6	0.12±0.11
		8	41.1	+1.9±3.4	0.05±0.08			53	5.5	+0.7±0.6	0.12±0.10
1007	1491–1532	6163	4.7	-2.0±0.7	0.43±0.16	2257	1537–1554	1318	14.3	-0.6±1.5	0.04±0.10
		1095	9.9	+8.4±1.0	0.85±0.12			129	14.4	-0.4±1.7	0.03±0.12
		5068	8.9	-10.4±0.9	1.17±0.12			1189	14.1	-0.2±1.4	0.01±0.10
						2357	1525–1541	103	12.8	-0.0±0.9	0.00±0.07

^a Truncated, see Table 1 for full name.

Table 4. BAL variability in RQQs

Coordinates	z	$\Delta\tau^a$	$\langle EW \rangle$	ΔEW	$\frac{ \Delta EW }{\langle EW \rangle}$	Ref	Coordinates	z	$\Delta\tau$	$\langle EW \rangle$	ΔEW	$\frac{ \Delta EW }{\langle EW \rangle}$	Ref
001130.5+005550	2.31	219	12.1	-0.7±1.4	0.06	G09	123355.6+130409	2.38	2411	30.5	+6.2±1.7	0.20	G10
001219.6+023636	2.64	2118	21.3	+17.9±2.2	0.84	G10	123458.1+130855	2.36	2038	60.6	-1.3±0.6	0.02	C11
001306.1+000431	2.16	1498	5.6	-3.5±1.5	0.63	G10	123724.5+010615	2.02	1680	6.1	-0.7±1.0	0.12	G10
001927.8+003359	1.62	276	15.6	-6.3±1.4	0.41	G09	123736.4+143640	2.70	1790	37.7	+4.2±3.2	0.11	G10
002127.8+010420	1.82	1571	12.4	+2.3±1.3	0.19	G10	123754.8+084106	2.90	2082	25.0	-3.0±1.7	0.12	G10
002227.5+012413	2.13	2447	27.8	+11.8±1.5	0.43	G10	124303.6+155047	2.36	2192	31.3	+6.3±1.7	0.20	G10
002410.8-015647	2.35	2118	45.3	+4.9±1.7	0.11	G10	124551.4+010505	2.81	2009	39.3	-4.9±2.6	0.13	G10
002435.3+020648	2.83	2045	13.2	-5.6±1.9	0.43	G10	124913.8-055919	2.25	1823	30.9	-0.4±0.5	0.01	C11
002733.8-013452	2.08	2484	21.5	-11.0±1.7	0.51	G10	130058.1+010551	1.91	105	43.0	+2.6±1.3	0.06	L07
003135.5+003421	2.25	2338	35.0	+6.0±1.8	0.17	G10	130554.7+303252	1.77	2104	39.9	+35.6±0.9	0.89	C11
003218.4+073832	3.25	89	7.2	-0.3±0.6	0.04	B93	131136.5-055239	2.16	1684	58.7	-3.3±0.4	0.06	C11
004118.5+001742	1.77	170	11.2	+0.4±1.4	0.04	G09	131305.7+015926	2.02	88	9.5	+1.6±0.4	0.17	L07
004527.6+143816	1.99	19	35.3	-0.4±0.3	0.01	L07	131714.2+010013	2.70	2082	32.1	+20.0±2.5	0.62	G10
005355.1-000309	1.72	1461	34.8	-11.5±1.4	0.33	G10	131853.4+002211	2.07	104	16.4	+1.3±0.6	0.08	L07
005824.7+004113	1.92	1498	5.2	-2.3±1.1	0.45	G10	132742.9+003532	1.88	103	3.8	+1.5±0.6	0.39	L07
011227.6-011221	1.76	1461	21.0	+16.9±1.2	0.80	G10	133901.8+132018	2.45	2016	42.2	-2.0±0.6	0.05	C11
011237.3+001929	2.66	523	4.0	+1.4±1.4	0.35	G09	134544.5+002810	2.45	80	18.3	+2.8±0.5	0.15	L07
011913.2+005115	1.67	157	24.6	+4.4±1.4	0.18	G09	142333.5+573909	1.87	547	18.8	-6.0±1.4	0.32	G09
012209.9+032544	2.09	2034	32.3	-3.3±1.6	0.10	C11	142500.2+494729	2.25	1801	20.6	-3.8±1.2	0.18	C11
013625.6-103346	2.01	487	26.5	-2.1±1.4	0.08	G09	143130.0+570138	1.80	31	16.8	-2.1±0.6	0.13	L07
014055.5+003908	1.49	167	10.0	+0.0±1.4	0.00	G09	143641.2+001558	1.87	18	23.1	+0.6±0.7	0.03	L07
014817.5+043119	2.03	281	21.6	+3.2±2.0	0.15	B93	143647.5+495256	1.59	2283	63.1	-6.9±2.0	0.11	C11
014918.7+015723	2.91	1695	42.7	-9.8±0.5	0.23	C11	143907.5-010616	1.82	265	7.2	+0.7±1.4	0.10	G09
020006.3-003709	2.14	575	52.3	+2.5±1.4	0.05	G09	144244.2-010943	1.93	256	9.1	+0.1±1.4	0.01	G09
022839.2-101111	2.26	1702	48.8	+5.5±0.3	0.11	C11	144403.9+565751	1.86	31	1.6	+0.5±0.3	0.32	L07
024413.7-000447	2.80	210	18.9	-5.9±1.4	0.31	G09	144514.8-002358	2.24	2301	38.5	+2.5±1.5	0.07	G10
024701.1+000330	2.15	350	9.1	-0.2±1.4	0.02	G09	144545.3+012912	2.45	2155	44.4	+0.9±1.7	0.02	G10
025042.4+003536	2.39	342	47.3	+0.2±1.4	0.00	G09	144959.9+003225	1.72	121	10.5	-0.2±0.6	0.02	L07
025751.5+002045	1.51	155	11.1	+1.2±1.4	0.11	G09	145428.5+571441	3.27	21	3.9	+0.9±0.5	0.22	L07
030504.9+171653	2.89	1614	12.9	+0.1±0.3	0.00	C11	150109.1-011502	2.13	120	23.2	-7.8±1.5	0.34	L07
031828.9-001523	1.98	36	3.1	+1.5±0.5	0.48	L07	151927.4-010729	1.72	265	11.5	+0.4±1.4	0.03	G09
075010.1+304032	1.89	109	3.2	-4.7±0.3	1.45	L07	152553.8+513649	2.88	1578	16.7	-2.6±0.2	0.16	C11
081416.7+435405	1.35	92	16.7	+2.4±1.4	0.14	L07	160649.2+451051	2.83	23	4.6	+1.1±0.7	0.23	L07
081657.5+060441	2.01	75	11.5	-5.1±1.7	0.44	L07	170114.3+222448	1.90	199	3.7	+1.2±1.4	0.32	G09
081822.6+434633	2.04	81	1.5	+2.7±0.3	1.82	L07	170633.0+615715	2.01	61	4.0	+0.8±0.3	0.20	L07
084538.6+342043	2.15	2023	24.5	-0.4±0.7	0.02	C11	172001.3+621245	1.76	34	23.0	-0.1±1.4	0.01	L07
084908.1+152931	2.93	1381	6.3	+1.6±0.3	0.26	C11	222830.4-051855	1.98	375	45.1	+4.8±1.9	0.11	B93
090638.1+172223	2.69	1841	66.0	-17.4±0.5	0.26	C11	224019.0+144435	2.24	79	1.9	-0.1±0.6	0.08	L07
093552.9+495314	1.93	2301	49.4	+1.7±0.5	0.04	C11	224320.4-004918	1.78	160	17.5	+9.7±1.4	0.55	G09
093620.5+004649	1.72	106	3.4	+5.2±0.7	1.50	L07	224324.5-005330	1.90	154	22.2	-5.6±1.4	0.25	G09
094425.4+610934	2.27	569	36.8	-2.8±1.4	0.08	G09	224733.4-002009	2.51	309	23.9	+1.8±1.4	0.08	G09
095933.6-054952	1.81	2082	18.8	+0.1±0.7	0.01	C11	225746.9+000121	1.73	298	5.8	+1.5±1.4	0.26	G09
101341.8+085126	2.27	1804	48.4	-0.2±1.1	0.01	C11	234315.8+004659	2.78	392	10.1	+0.7±1.4	0.07	G09
102250.1+483631	2.07	107	27.7	-2.7±0.6	0.10	L07	234506.3+010135	1.80	231	32.2	+2.9±1.4	0.09	G09
112820.8-011441	1.80	272	13.8	+1.3±1.4	0.09	G09	235224.1-000951	2.74	197	20.7	+3.4±1.4	0.16	G09
115031.0-004403	2.39	83	11.6	+0.3±1.6	0.03	L07	235253.5-002850	1.62	281	30.1	+3.4±1.4	0.11	G09
121125.4+151851	1.96	2228	28.7	+6.4±1.6	0.22	G10	235408.6-001615	1.77	265	41.8	-12.1±1.4	0.29	G09

^a These and following columns defined as in Table 1.

Table 5. BAL variability in RLQs and RQQs

Sample	n	$\Delta\tau$ (d)			$\langle EW \rangle$ (Å)			$ \Delta EW $ (Å)			$ \Delta EW /\langle EW \rangle$		
		Med	Mean	KS p	Med	Mean	KS p	Med	Mean	KS p	Med	Mean	KS p
Groupings of RLQs													
All values	78	473	665±108	...	14.5	20.7±1.6	...	1.0	1.9±0.3	...	0.06	0.12±0.02	...
Longest sep	46	503	724±143	...	12.8	18.6±2.2	...	1.0	1.7±0.4	...	0.06	0.12±0.02	...
Core dom	39	465	579± 87	...	14.5	19.9±2.4	...	0.7	1.7±0.5	...	0.04	0.09±0.02	...
Lobe dom	7	770	1532±778	0.04	7.8	11.4±5.0	0.01	1.8	1.8±0.3	0.05	0.22	0.24±0.07	0.04
$\ell_r < 33$	24	319	726±262	...	15.4	21.1±3.2	...	1.1	1.6±0.4	...	0.06	0.09±0.02	...
$\ell_r \geq 33$	22	624	723± 95	0.01	11.6	15.8±3.0	0.21	1.0	1.8±0.7	1.00	0.05	0.15±0.04	0.96
$R^* < 2$	30	419	519±106	...	15.0	20.8±3.1	...	1.0	1.8±0.6	...	0.04	0.10±0.03	...
$R^* \geq 2$	16	745	1110±346	0.00	11.6	14.4±2.8	0.28	1.4	1.4±0.3	0.54	0.06	0.15±0.04	0.52
Groupings of RQQs													
All values	115	281	808± 80	...	21.6	24.7±1.5	...	2.1	3.6±0.5	...	0.11	0.21±0.03	...
Longest sep	94	350	921± 92	...	21.0	23.2±1.7	...	2.5	4.1±0.5	...	0.13	0.24±0.03	...
Lundgren+07	24	81	72± 7	0.00	11.5	13.2±2.3	0.01	1.5	2.0±0.4	0.20	0.17	0.35±0.10	0.69
Gibson+09	28	265	296± 25	0.00	17.5	19.6±2.5	0.38	1.8	2.8±0.6	1.00	0.10	0.16±0.03	0.76
Capellupo+11	18	1841	1878± 59	0.00	42.2	37.9±4.3	0.04	2.6	5.3±2.1	0.98	0.10	0.14±0.05	0.53
Gibson+10	21	2082	1999± 75	0.00	28.7	26.5±2.7	0.26	5.6	7.1±1.2	0.00	0.20	0.32±0.05	0.02
Comparison of RLQs to RQQs (for $EW > 3.5$ Å, longest separation)													
RLQs	42	503	740±155	...	14.5	20.1±2.3	...	1.0	1.8±0.5	...	0.05	0.10±0.02	...
RQQs	88	487	978± 96	0.00	21.6	24.6±1.7	0.02	2.5	4.2±0.6	0.00	0.12	0.19±0.02	0.00
RQQs matched	42	375	738±106	0.26	18.8	22.1±2.3	0.56	2.3	3.3±0.6	0.01	0.11	0.17±0.03	0.01
RLQs $EW < 20$ Å	28	512	736±214	...	11.7	11.2±0.7	...	0.7	1.1±0.2	...	0.06	0.10±0.02	...
RQQs $EW < 20$ Å	39	219	529±104	0.01	11.1	10.8±0.8	0.33	1.3	2.0±0.3	0.17	0.15	0.19±0.03	0.07
RLQs $EW \geq 20$ Å	14	496	749±194	...	39.9	37.9±3.4	...	1.4	3.2±1.2	...	0.04	0.09±0.04	...
RQQs $EW \geq 20$ Å	49	1790	1336±130	0.05	32.3	35.6±1.7	0.58	3.4	5.9±0.9	0.00	0.11	0.19±0.03	0.01
RLQs $\Delta\tau < 500$ d	21	130	233± 39	...	16.2	21.2±3.3	...	0.8	1.0±0.2	...	0.04	0.06±0.02	...
RQQs $\Delta\tau < 500$ d	45	160	180± 17	0.10	16.4	18.1±1.7	0.67	1.5	2.4±0.4	0.03	0.11	0.15±0.02	0.01
RLQs $\Delta\tau \geq 500$ d	21	854	1247±268	...	11.7	19.0±3.3	...	1.4	2.5±0.9	...	0.06	0.13±0.03	...
RQQs $\Delta\tau \geq 500$ d	43	2009	1814± 77	0.00	31.3	31.4±2.5	0.00	3.5	6.0±1.1	0.00	0.16	0.23±0.04	0.10

Note: The median and mean values are given for each grouping; the error on the mean is σ/\sqrt{n} . The KS-test probability is versus the nearest preceding grouping without entered values, and $p < 0.005$ ($p \geq 0.995$) are represented as 0.00 (1.00).

Table 6. Correlation tests

Sample	n	p_τ	p_ρ	$ \Delta EW $		β	$ \Delta EW /\langle EW \rangle$			
				ρ			p_τ	p_ρ	ρ	β
Versus $\Delta\tau$										
RLQs, all values	78	0.99	0.99	0.30	0.47±0.23		0.99	0.99	0.31	0.36±0.14
RLQs, longest sep	46	0.97	0.97	0.32	0.50±0.28		0.96	0.95	0.29	0.72±0.28
RLQs, $EW > 3.5\text{\AA}$	42	0.97	0.97	0.34	0.53±0.29		0.97	0.96	0.32	0.68±0.26
RLQs, core dom	39	0.81	0.81	0.21	0.24±0.29		0.81	0.79	0.20	0.14±0.16
RLQs, lobe dom	7	0.64	0.60	0.38	1.46±0.71		0.35	0.30	0.18	1.77±2.03
RQQs, all values	115	1.00	1.00	0.36	1.55±0.40		0.44	0.42	0.05	0.39±0.24
RQQs, longest sep	94	1.00	1.00	0.40	1.81±0.48		0.03	0.03	0.00	0.31±0.28
RQQs, $EW > 3.5\text{\AA}$	88	1.00	1.00	0.39	1.93±0.53		0.67	0.67	0.10	0.45±0.28
RQQs, matched	42	0.99	0.99	0.40	1.47±0.63		0.96	0.96	0.32	1.04±0.40
RQQs+RLQs $EW > 3.5\text{\AA}$	130	1.00	1.00	0.39	1.29±0.34		0.97	0.97	0.19	0.52±0.21
Versus $\langle EW \rangle$										
RLQs, all values	78	1.00	1.00	0.34	0.29±0.10		0.87	0.90	-0.19	-0.01±0.01
RLQs, longest sep	46	0.98	0.98	0.34	0.15±0.11		0.93	0.92	-0.26	-0.01±0.01
RLQs, $EW > 3.5\text{\AA}$	42	0.97	0.97	0.34	0.14±0.12		0.75	0.71	-0.17	-0.01±0.01
RLQs, core dom	39	1.00	1.00	0.47	0.23±0.08		0.51	0.51	-0.11	0.00±0.01
RLQs, lobe dom	7	0.64	0.64	0.41	0.06±0.28		0.35	0.36	-0.21	-0.07±0.05
RQQs, all values	115	1.00	1.00	0.30	0.41±0.15		1.00	1.00	-0.34	-0.03±0.01
RQQs, longest sep	94	1.00	1.00	0.40	0.71±0.19		1.00	1.00	-0.29	-0.02±0.01
RQQs, $EW > 3.5\text{\AA}$	88	1.00	1.00	0.42	0.76±0.21		0.94	0.94	-0.20	-0.02±0.01
RQQs, matched	42	0.98	0.99	0.38	0.74±0.24		0.83	0.81	-0.20	-0.02±0.02
RQQs+RLQs $EW > 3.5\text{\AA}$	130	1.00	1.00	0.43	0.65±0.13		0.83	0.82	-0.12	-0.02±0.01
Versus optical continuum variability										
RLQs, longest sep	44	0.25	0.14	0.03	0.11±0.21		0.69	0.63	0.14	0.17±0.17
RLQs, core dom	39	0.17	0.08	0.15	0.15±0.26		0.81	0.74	0.19	0.35±0.14
RLQs, lobe dom	7	0.14	0.10	-0.06	-0.03±0.35		0.41	0.42	-0.26	-0.62±0.68
RQQs, longest sep	90	0.11	0.09	0.01	0.00±0.53		0.71	0.71	0.11	0.10±0.29
RQQs, matched	45	0.53	0.50	0.10	-0.10±0.62		0.48	0.49	0.10	0.26±0.41
RQQs+RLQs	134	0.59	0.54	0.06	-0.01±0.32		0.92	0.91	0.15	0.12±0.20
Versus ℓ_r (RLQs only)										
RLQs, longest sep	46	0.21	0.21	-0.04	0.00±0.24		0.14	0.14	0.03	0.14±0.24
RLQs, $EW > 3.5\text{\AA}$	42	0.13	0.14	-0.03	0.04±0.25		0.07	0.07	-0.01	0.06±0.21
RLQs, $3.5 < EW < 20\text{\AA}$	28	0.40	0.28	0.07	0.27±0.29		0.46	0.43	0.11	0.27±0.29
RLQs, $EW \geq 20\text{\AA}$	14	0.91	0.86	-0.42	-0.55±0.39		0.68	0.64	-0.27	-0.32±0.20
RLQs, $\Delta\tau < 500$ d	21	0.10	0.08	-0.02	-0.15±0.31		0.67	0.66	-0.22	-0.22±0.20
RLQs, $\Delta\tau \geq 500$ d	21	0.36	0.35	-0.11	0.09±0.40		0.02	0.02	0.01	0.09±0.45
Versus R^* (RLQs only)										
RLQs, longest sep	46	0.32	0.25	-0.05	0.17±0.27		0.45	0.49	0.10	0.35±0.27
RLQs, $EW > 3.5\text{\AA}$	42	0.33	0.29	-0.06	0.21±0.30		0.03	0.09	0.02	0.22±0.25
RLQs, $3.5 < EW < 20\text{\AA}$	28	0.77	0.74	0.22	0.66±0.33		0.80	0.81	0.25	0.68±0.35
RLQs, $EW \geq 20\text{\AA}$	14	0.99	0.99	-0.70	-0.54±0.41		0.92	0.92	-0.48	-0.29±0.21
RLQs, $\Delta\tau < 500$ d	21	0.55	0.44	-0.13	-0.28±0.43		0.59	0.52	-0.16	-0.21±0.26
RLQs, $\Delta\tau \geq 500$ d	21	0.46	0.43	-0.13	0.31±0.46		0.10	0.10	-0.03	-0.00±0.47

Note: The probabilities p_τ and p_ρ are for the Kendall's and Spearman tests, and ρ is the Spearman correlation coefficient. The slope β is calculated using the IDL routine `robust_linefit` and for the linear regression $\Delta\tau$ is expressed as a logarithm, $|\Delta EW|/\langle EW \rangle$ is multiplied by 10 for all fits, and $|\Delta EW|$ is multiplied by 10 only versus $\langle EW \rangle$.

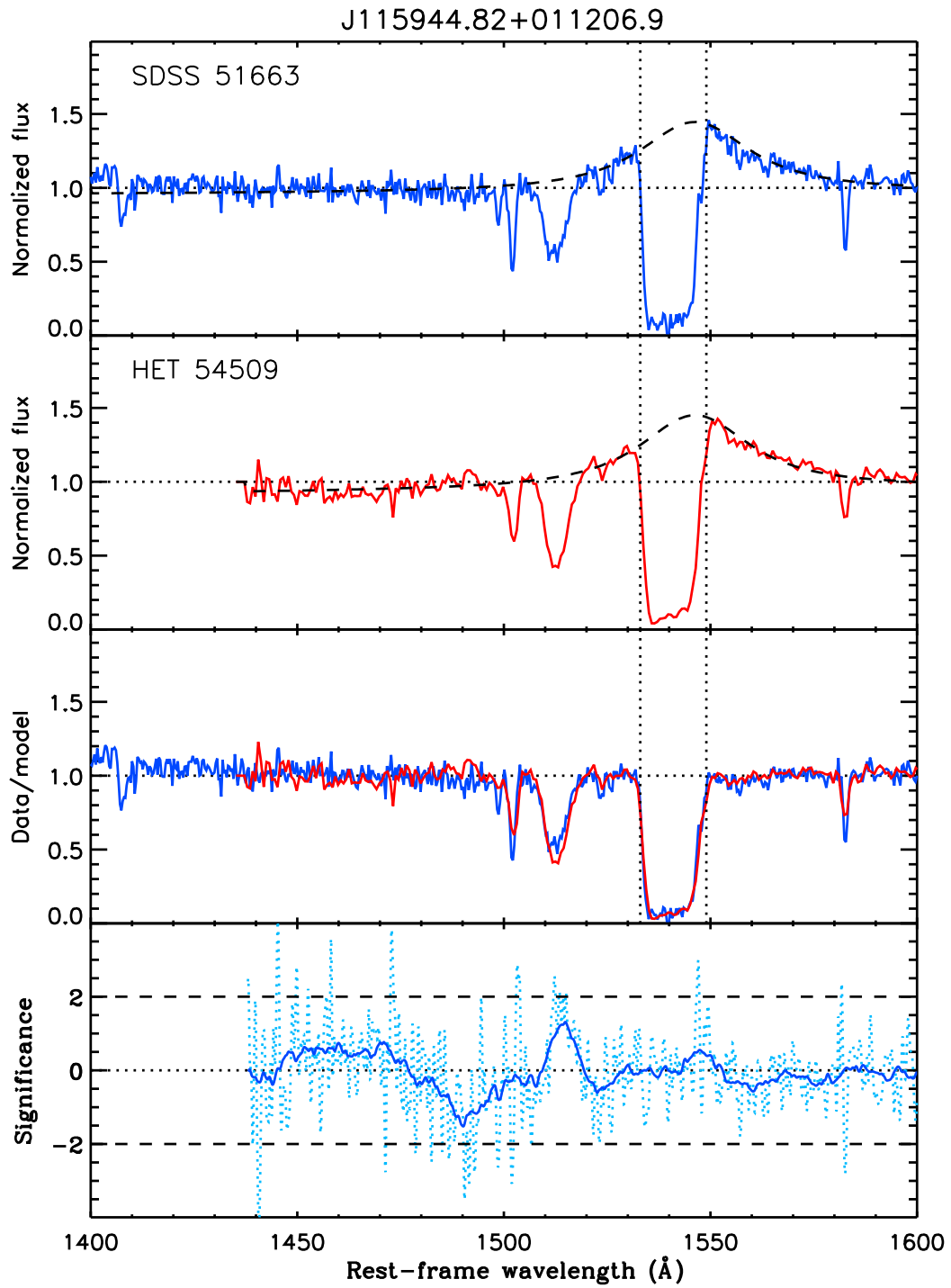


Figure 1. Appendix A: Assessment of BAL variability for 115944.82+011206.9, as in Figure 4. (Selected example, full Appendix A has all BAL RLQs spectra used in this work.)

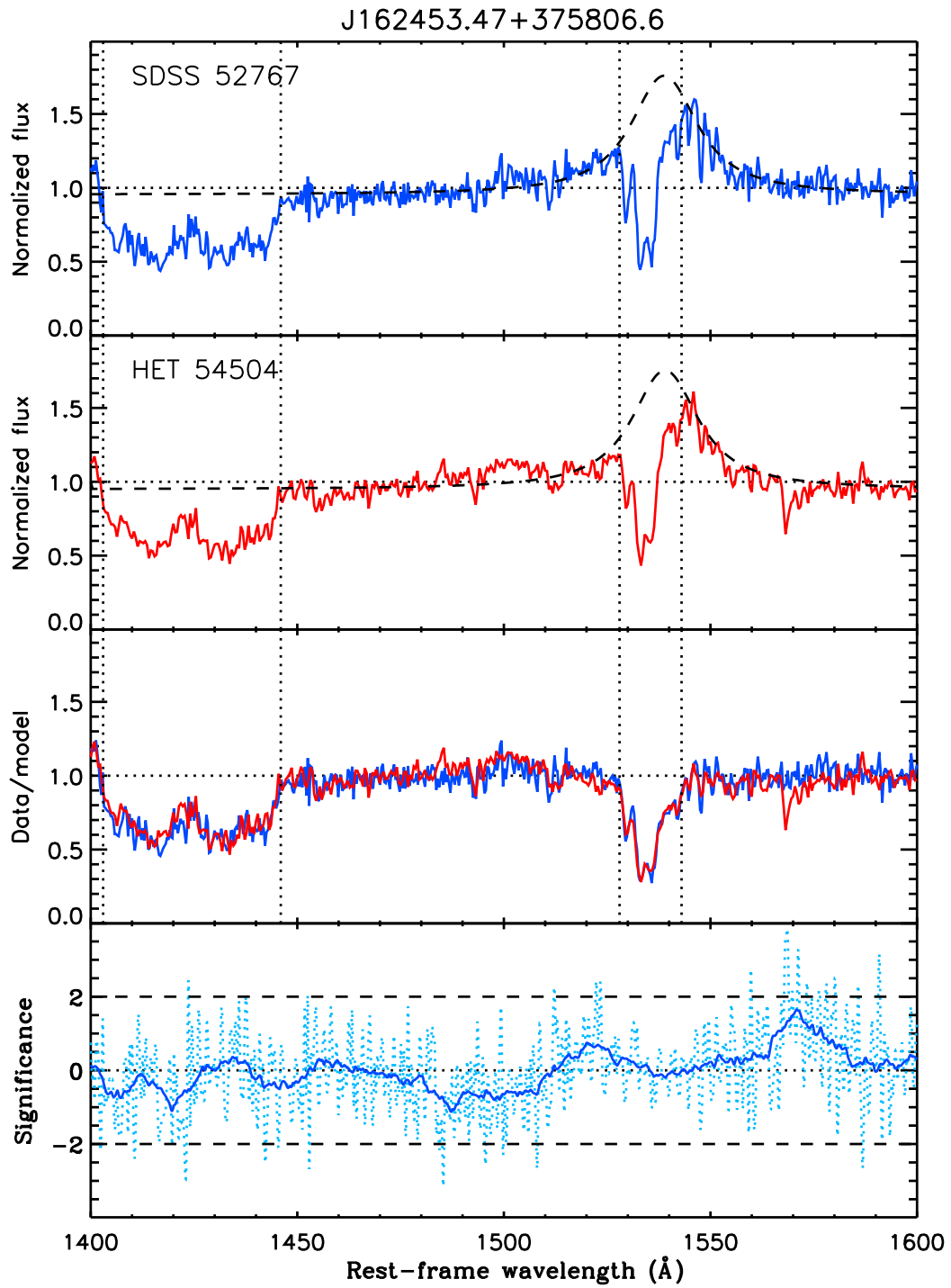


Figure 2. Appendix A: Assessment of BAL variability for 162453.47+375806.6, as in Figure 4. (Selected example, full Appendix A has all BAL RLQs spectra used in this work.)

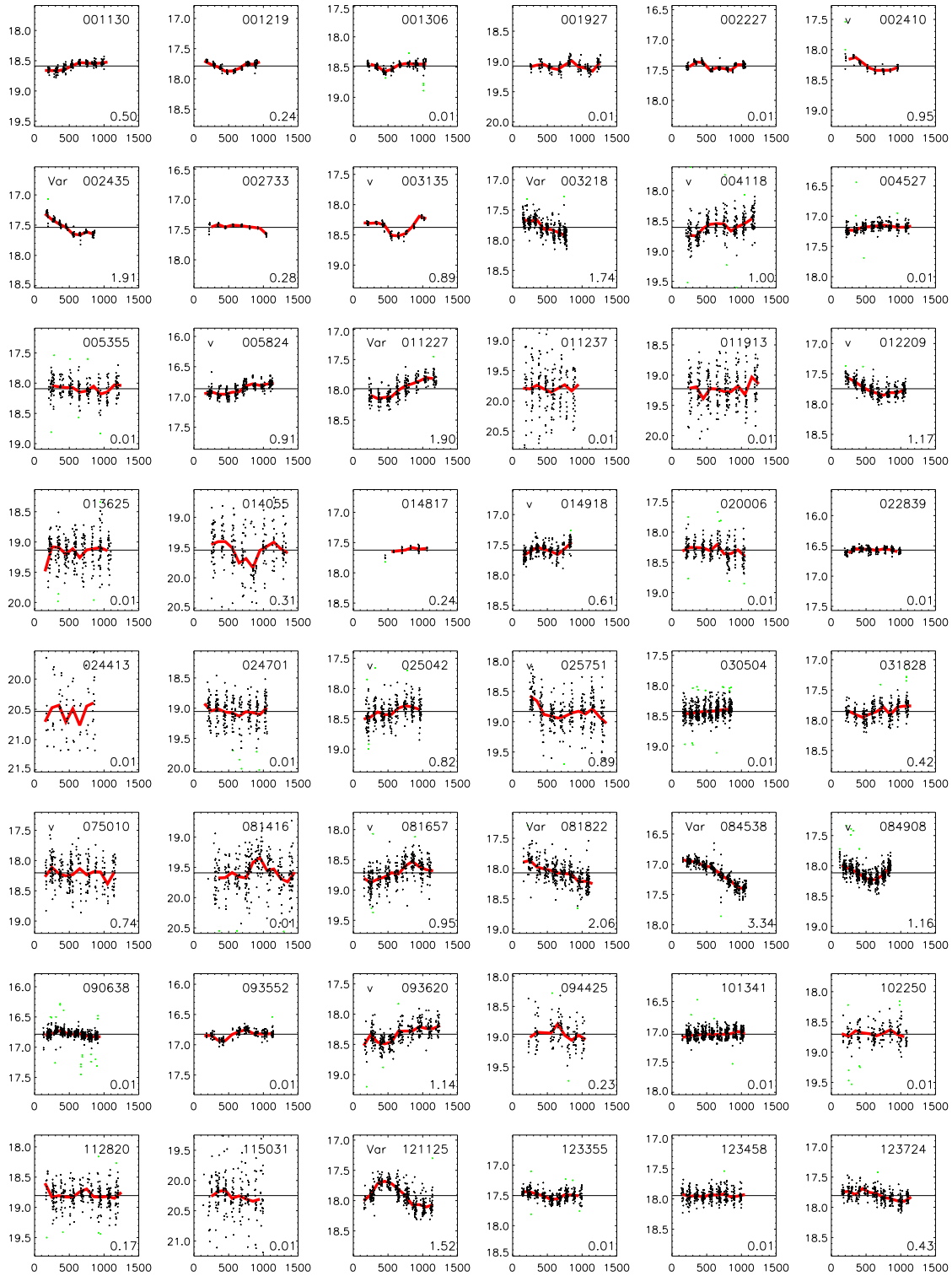


Figure 1. Appendix B: Optical continuum variability for first set of BAL RQs, as in Figure 13.

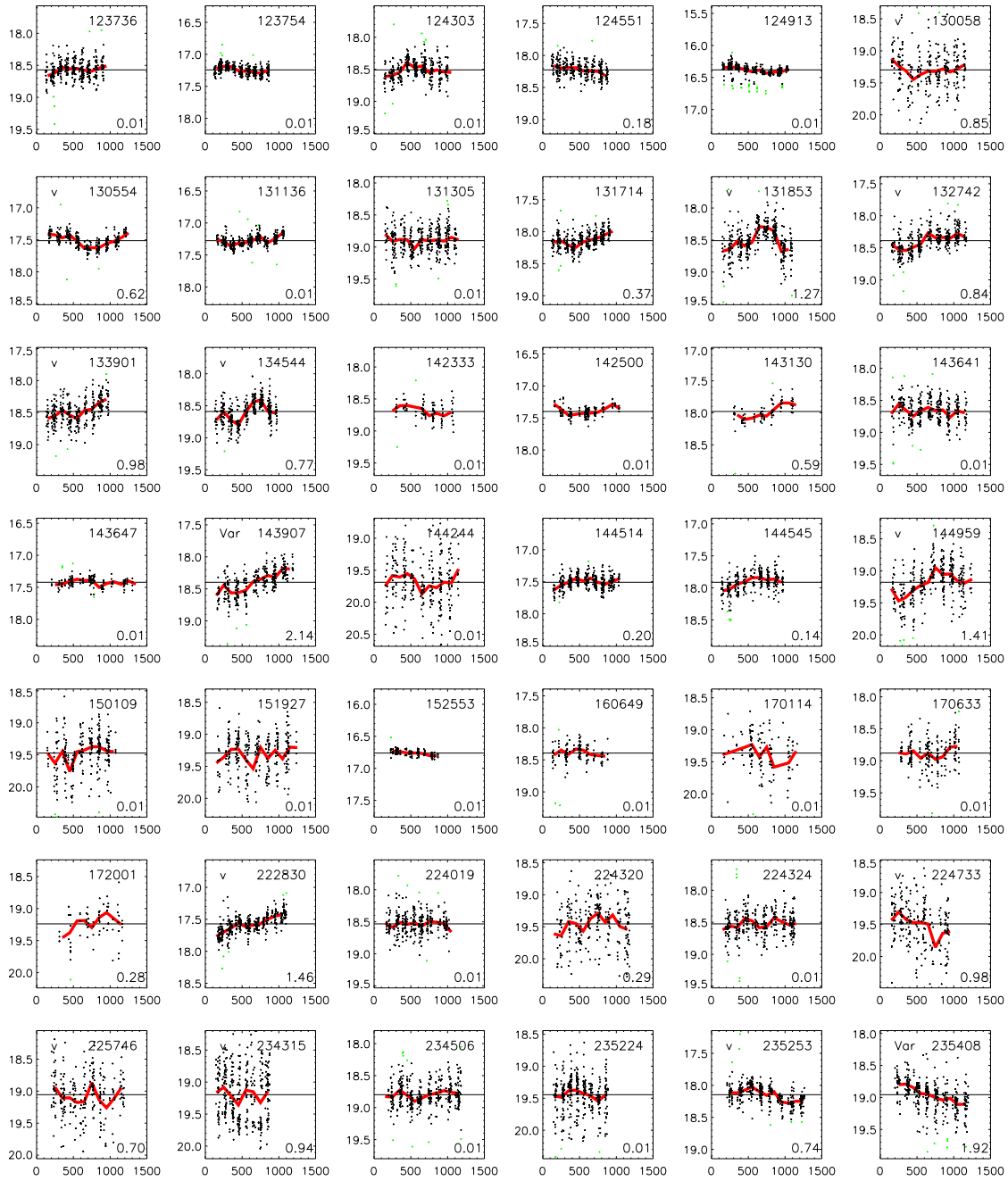


Figure 2. Appendix B: Optical continuum variability for second set of BAL RQQs, as in Figure 13.